Prepared for submission to JCAP

Lattice simulations of axion-U(1) inflation: gravitational waves, magnetic fields, and black holes

Ramkishor Sharma,[a] **Axel Brandenburg,**[b,c,d,e] **Kandaswamy Subramanian,**[f,g] **and Alexander Vikman**[a]

[a]CEICO, FZU-Institute of Physics of the Czech Academy of Sciences, Na Slovance 1999/2, 182 00 Prague 8, Czech Republic

[b]Nordita, KTH Royal Institute of Technology and Stockholm University, Hannes Alfvéns väg 12, 10691 Stockholm, Sweden

[c]The Oskar Klein Centre for Cosmoparticle Physics, Department of Physics, Stockholm University, AlbaNova, 10691 Stockholm, Sweden

[d]McWilliams Center for Cosmology & Department of Physics, Carnegie Mellon University, Pittsburgh, PA 15213, USA

[e]School of Natural Sciences and Medicine, Ilia State University, 3-5 Cholokashvili Avenue, 0194 Tbilisi, Georgia

[f]IUCAA, Post Bag 4, Ganeshkhind, Pune 411007, India

[g]Department of Physics, Ashoka University, Rajiv Gandhi Education City, Rai, Sonipat 131029, Haryana, India

E-mail: sharma@fzu.cz, brandenb@nordita.org, kandu@iucaa.in, vikman@fzu.cz

Abstract. We numerically study axion-U(1) inflation, focusing on the regime where the coupling between axions and gauge fields results in significant backreaction from the amplified gauge fields during inflation. These amplified gauge fields not only generate high-frequency gravitational waves (GWs) but also induce spatial inhomogeneities in the axion field, which can lead to the formation of primordial black holes (PBHs). Both GWs and PBHs serve as key probes for constraining the coupling strength between the axion and gauge fields. We find that, when backreaction is important during inflation, the constraints on the coupling strength due to GW overproduction are relaxed compared to previous studies, in which backreaction matters only after inflation. For PBH formation, understanding the probability density function (PDF) of axion field fluctuations is crucial. While earlier analytical studies assumed that these fluctuations followed a χ^2-distribution, our results suggest that the PDF tends toward a Gaussian distribution in cases where gauge field backreaction is important, regardless whether during or after inflation. We also calculate the spectrum of the produced magnetic fields in this model and find that their strength is compatible with the observed lower limits.

Contents

1 Introduction

The idea of inflation originated from attempts to solve the singularity problem [1] and to address the horizon, isotropy and flatness problems in the hot big bang along with the monopole problem of grand unification, see [2–4] and [5, 6]. Inflation not only ameliorates the latter set of issues, but most importantly provides a natural mechanism [7–9] for generating initial density perturbations in the universe from mere vacuum fluctuations, see also [10–13]. These perturbations account for anisotropies in the cosmic microwave background radiation (CMB) recently measured by Planck collaboration [14] with unprecedented precision, thereby confirming the predictions of this mechanism and the theory of inflation. Later on these perturbations collapse to form all galaxies and the large-scale structure in the universe.

Following the initial proposal, numerous models have been suggested to realize an inflationary era in the early universe (for details see refs. [15–19]). Axion inflation models are particularly interesting because they provide a natural high energy physics ingredient for a long lasting inflation - an approximate shift symmetry of the potential [20]. After the first proposal, several models have been suggested in the context of axion inflation [21–28]; see ref. [29] for a review. One of these models [25] considers a coupling of the axion field with the U(1) gauge field and we focus on this model in this paper. The axion inflation model, where the axion couples to a gauge field, exhibits a rich phenomenology. This includes the production of gravitational waves (GWs) [30–36], primordial black holes (PBHs) [37–39], matter-antimatter asymmetry [40, 41], and primordial magnetic fields [42–49]. The rich phenomenology of axion inflation has prompted extensive studies to understand the dynamics of these models. In scenarios with a sufficiently strong coupling between the axion and the gauge field, the backreaction of the produced gauge fields becomes important either during inflation or post inflation depending on the coupling strength. This model including the backreaction of the gauge fields has been studied semi-analytically through perturbative approaches [50–52] and the gradient expansion formalism (GEF) [49, 53] under the assumption of a homogeneous axion field. More recently, efforts have been made to numerically investigate the strong backreaction regime, where the assumption of homogeneous axion field is relaxed [54–56]. Motivated by the importance of inhomogeneities of the axion field, as demonstrated in the numerical studies, these inhomogeneities have also been incorporated perturbatively into GEF [57].

This rich phenomenology of axion inflation has been used to constrain the coupling strength between the axion and gauge fields. The coupling between the axion and the gauge field results in the production of gauge fields, which in turn generate high-frequency GWs, typically in the GHz range [35, 36]. These GWs contribute to the early universe's total energy budget as additional radiation degrees of freedom. The bound on additional radiation degrees of freedom from CMB observations constrains the produced GWs, which further limits the coupling between the axion and the gauge fields. We reexamine the bounds on the coupling strength between the axion and the gauge field, considering stronger couplings than those explored in previous works [35, 36]. In [35], the authors considered scenarios where the backreaction due to the produced gauge field became important in the post-inflationary era but not during inflation. For one of their models, the chaotic inflation model, they found that the coupling strength should be below $(m_{\rm pl}/70)^{-1}$ for an inflaton mass equal[1] to $1.2\times10^{-6}m_{\rm pl}$. In our study, we explore scenarios with larger coupling strengths, where the gauge field energy density becomes large enough to affect the duration of inflation. Corresponding studies in refs. [54, 55] did not address the production of GWs, however. In these scenarios, inflation ends when the gauge field energy density becomes comparable to the inflaton field's potential energy. Our findings indicate that in such scenarios, the bounds on the coupling strength are relaxed compared to previous estimates [35, 36].

Additionally, the produced gauge field can also enhance spatial fluctuations of the axion field. If these spatial fluctuations exceed a threshold value, they can lead to the formation of PBHs[2] in the post-inflationary era. This phenomenon has been analyzed in detail considering the χ^2-distribution of the spatial fluctuations of the axion field. Given that the backreaction of the gauge field on the axion field is quadratic in nature, and assuming the gauge field has a Gaussian distribution, the spatial fluctuations of the axion field are expected to follow a χ^2-

[1] Here and throughout the paper $m_{\rm pl} = 1.22 \times 10^{19}$ GeV represents the Planck mass.

[2] For other models of the formation of PBHs during inflation see, e.g., refs. [58–62].

distribution. By using constraints on PBH abundances, a bound on the axion and gauge field coupling has been obtained [37, 38]. A recent numerical study of axion inflation [54] considers the case when the backreaction of the gauge field on the axion evolution becomes significant during inflation. It was found that the distribution of the spatial fluctuations of the axion field starts to deviate from the χ^2-distribution and begins to resemble a Gaussian distribution. In this paper, we study the probability distribution of spatial fluctuations in the axion field over a range of coupling strengths. We find that the distribution tends to a χ^2-distribution during the evolution. However, it gradually transitions to a Gaussian distribution at a later time, irrespective of whether the backreaction of the gauge fields becomes important during or after inflation.

The paper is organized as follows. In section 2, we discuss the axion-inflation model and state the governing evolution equations for this system. In section 3, we describe the initial conditions of our numerical simulations, present the simulation results, and compare them with previous semi-analytical studies. The production of GWs considered in section 4. The magnetic part of the produced gauge fields may explain the presence of magnetic fields in the intergalactic medium, which we discuss in section 5. In section 6, we describe the probability density function of the curvature perturbation. In section 7, we present the conclusions of our study.

Throughout this paper, the indices i, j, k represent three-dimensional vector indices, and the background spacetime metric is assumed to be the spatially-flat Friedmann-Lemaitre-Robertson-Walker (FLRW) metric. Capital bold letters denote three-dimensional vector quantities. We use signature convention $(-,+,+,+)$ and Planck units $\hbar = c = G = 1$. The Planck mass is defined as $m_{\rm pl} = 1/\sqrt{G}$.

2 Axion-U(1) inflation model

The following action describes the dynamics of the axion-U(1) inflation model,

$$S = \int d^4x\sqrt{-g}\left[\frac{m_{\rm pl}^2}{16\pi}R - \frac{1}{2}\partial_\mu\phi\partial^\mu\phi - V(\phi) - \frac{1}{4}F_{\mu\nu}F^{\mu\nu} - \frac{\alpha}{4f}\phi F_{\mu\nu}\tilde{F}^{\mu\nu}\right]. \tag{2.1}$$

Here, ϕ represents the axion field and $V(\phi)$ denotes its potential, which in our analysis is taken as[3] $V(\phi) = m^2\phi^2/2$ with $m = 1.06\times10^{-6}m_{\rm pl}$, $F_{\mu\nu} = \partial_\mu A_\nu - \partial_\nu A_\mu$ represents the gauge field strength tensor,[4] while $\tilde{F}^{\mu\nu}$ is its Hodge dual, α/f denotes the coupling strength between the axion field and the U(1) gauge fields, and R is the Ricci scalar. Using this, and denoting derivatives with respect to conformal time η by a prime, we get the following

[3] Although chaotic inflation has been ruled out by CMB observations [18], we have chosen this model for several reasons. First, it simplifies our analysis. Second, it allows us to compare our results directly with those of previous studies. Lastly, many other inflationary potentials can be approximated by a quadratic potential near the end of inflation, and our study primarily focuses on this late phase of the inflationary period.

[4] In this work, we identify the gauge fields with the Standard Model hypercharge sector. The production of fermions is important in this context [49, 63], but their numerical modeling touches upon many unsolved questions, which we have to leave for future work. Alternatively, the scenario in this study could apply to gauge fields in a dark sector, but in that case, these dark sector gauge fields would not provide magnetogenesis as discussed in section 5.

dynamical equations[5] for the axion-gauge field evolution [45]

$$\phi'' + 2\mathcal{H}\phi' - \nabla^2\phi + a^2\frac{dV}{d\phi} = \frac{\alpha}{f}\frac{1}{a^2}\,\mathbf{E}\cdot\mathbf{B}\,, \tag{2.2}$$

$$\mathbf{A}'' - \boldsymbol{\nabla}A_0' - \nabla^2\mathbf{A} + \boldsymbol{\nabla}(\boldsymbol{\nabla}\cdot\mathbf{A}) - \frac{\alpha}{f}\left(\phi'\mathbf{B} + \boldsymbol{\nabla}\phi\times\mathbf{E}\right) = 0\,, \tag{2.3}$$

where[6] $\mathbf{E} = -\mathbf{A}' + \boldsymbol{\nabla}A_0$, $\mathbf{B} = \boldsymbol{\nabla}\times\mathbf{A}$ and $\mathcal{H}$ is the comoving Hubble parameter with $\mathcal{H} = a'/a$ for scale factor $a(\eta)$. On top of the constraint $\boldsymbol{\nabla}\cdot\mathbf{B} = 0$, the action (2.1) modifies the Coulomb law to

$$\boldsymbol{\nabla}\cdot\mathbf{E} + \frac{\alpha}{f}\mathbf{B}\cdot\boldsymbol{\nabla}\phi = 0\,. \tag{2.4}$$

Finally, the gravitational background obeys the Friedmann equations

$$\mathcal{H}^2 = \frac{8\pi}{3m_{\rm pl}^2}a^2\rho\,, \qquad \mathcal{H}' = -\frac{4\pi a^2}{m_{\rm pl}^2}(\rho + p) + \mathcal{H}^2\,, \tag{2.5}$$

where the density ρ and pressure p are given by [36]

$$\rho = \left\langle \frac{1}{2}\frac{\phi'^2}{a^2} + \frac{1}{2}\frac{(\boldsymbol{\nabla}\phi)^2}{a^2} + V(\phi) + \frac{\mathbf{E}^2 + \mathbf{B}^2}{2a^4}\right\rangle, \tag{2.6}$$

$$p = \left\langle \frac{1}{2}\frac{\phi'^2}{a^2} - \frac{1}{6}\frac{(\boldsymbol{\nabla}\phi)^2}{a^2} - V(\phi) + \frac{\mathbf{E}^2 + \mathbf{B}^2}{6a^4}\right\rangle, \tag{2.7}$$

and the $\langle..\rangle$ represents the spatial averaging over a cubic domain of size L^3, where $L = 2\pi/k_1$ is specified in terms of the lowest wave number of the domain, k_1. We consider different values for L, depending on the value of α/f.

Before turning to the numerical results, it is useful to discuss here the possibility of gauge field amplification in the case of a homogeneous axion field. By assuming a homogeneous axion field ($\boldsymbol{\nabla}\phi = 0$) and using the Coulomb gauge ($\boldsymbol{\nabla}\cdot\mathbf{A} = 0$), equation (2.4) implies $A_0 = 0$ and equation (2.3) reduces to,

$$\mathbf{A}'' - \nabla^2\mathbf{A} - \frac{\alpha}{f}\phi'\boldsymbol{\nabla}\times\mathbf{A} = 0\,. \tag{2.8}$$

By choosing the circular polarization basis, the above equation simplifies to the following form in Fourier space,

$$\left(\partial_\eta^2 + k^2 \mp 2\xi(\mathcal{H}\eta)\frac{k}{\eta}\right)A_k^\pm = 0\,, \qquad \text{where} \qquad \xi = -\frac{\alpha}{2f}\frac{\phi'}{\mathcal{H}}\,. \tag{2.9}$$

The above equation indicates that, as ϕ rolls down its potential, one of the modes of the gauge field amplifies depending on the velocity of the axion field ($\phi'/\mathcal{H}$) and the coupling strength (α/f). This phenomenon has been extensively discussed in the literature [42, 44, 45, 49]. For

[5] In this paper, we neglect the role of metric perturbations. The terms that couple metric perturbations to the axion field are suppressed by slow-roll parameters and can thus be ignored during inflation [64, 65]. However, the role of these terms may become important near the end of inflation, which we leave for future investigation; see refs. [56, 66, 67] for recent studies on this topic.

[6] We follow here the standard sign convention between $\mathbf{E}$ and $\mathbf{A}'$ [25], which differs from that of some other papers [45, 55].

large coupling strengths, the backreaction from the produced gauge fields becomes significant and must be considered, as it alters the dynamics of the system. This backreaction provides an additional friction term for the axion field evolution, leading to an extended duration of inflation compared to cases where backreaction is neglected.

In this paper, we use the Pencil Code [68] to solve these equations on a lattice in the regime where the backreaction from the produced gauge fields is significant; see appendix A for details about the implementation of these equations.

3 Numerical simulations of axion-U(1) inflation

3.1 Initial conditions

In this section, we describe the initial conditions for the axion and gauge fields used in our simulations. The initial conditions are set well within the inflationary era. To achieve accelerated expansion of the universe, the pressure p must satisfy $p < -\rho/3$ which in the absence of gauge field implies $\phi'^2 < a^2 V(\phi)$. Using this condition in its extreme form of $\ll$ in equations (2.5), we get

$$\mathcal{H}^2 \approx \frac{8\pi}{3m_{\rm pl}^2} a^2 V(\phi) \quad \text{and} \quad \epsilon_H \equiv -\frac{\dot{H}}{H^2} \approx \frac{3}{2}\frac{\phi'^2}{a^2 V(\phi)}\,, \tag{3.1}$$

here $H = \dot{a}/a = \mathcal{H}/a$ is the usual Hubble parameter, dot denotes derivative with respect to cosmological time $dt = a d\eta$ and ϵ_H represents the first slow-roll parameter. The above expressions imply

$$\phi' \approx a\sqrt{\frac{2\epsilon_H}{3} V(\phi)}\,. \tag{3.2}$$

Assuming $a = -1/(H\eta)$ during inflation, we get $\eta = -1/(aH) = -1/\mathcal{H}$, and thus the initial values of ϕ and η_i as

$$\phi_0'(\eta_i) = a_i\sqrt{\frac{2\epsilon_H}{3} V(\phi_{in})}, \quad \eta_i = -\frac{1}{\mathcal{H}_i}\,. \tag{3.3}$$

Here $\mathcal{H}_i = \sqrt{[8\pi/(3m_{\rm pl}^2)]V(\phi_0)}$ and ϕ_0 is the initial value of the homogeneous part of the axion field. For the quadratic inflation model, $V(\phi) = m^2\phi^2/2$, we have $\epsilon_H = 2/(8\pi\phi^2)$. This implies,

$$\phi_0'(\eta_i) = a_i \frac{m\ m_{\rm pl}}{\sqrt{12\pi}}\,. \tag{3.4}$$

In our simulations, we choose the initial condition for the axion field and its derivative such that

$$\phi(\eta_i) = \phi_0(\eta_i) + \delta\phi(\eta_i, \mathbf{x})\,, \tag{3.5}$$

$$\phi'(\eta_i) = \phi_0'(\eta_i) + \delta\phi'(\eta_i, \mathbf{x})\,, \tag{3.6}$$

where $\delta\phi$ represents the fluctuations arising from the quantum mechanical nature of the axion field. We initialize these fluctuations as a Gaussian random field with a power spectrum, $P_{\delta\phi}(k) = \mathcal{H}^2/2k^3\,(k/\mathcal{H})^2$ corresponding to the Bunch-Davies initial condition. At the

Run	α/f (in $m_{\rm pl}^{-1}$)	$\alpha/(\sqrt{8\pi}f)$	k_p/m	k_1/m	grid size	ΔN_e
A	35	7	47	2	512	0.0
B	50	10	47	2	512	0.0
C	60	12	47	2	512	0.0
D	75	15	47	4	1024	1.7
D'	75	15	94	2	512	1.7
E	90	18	47	8	1024	4.0

Table 1: Parameters for the runs discussed in the paper. Here k_1 represents the lowest wave number of the simulation domain and k_p is the cutoff wavenumber for the initial spectrum. ΔN_e denotes the excess number of e-folds over the case without backreaction due to the gauge fields.

beginning of our simulation, the chosen box size ensures that all wave numbers are within the Hubble horizon. To avoid the effects of large ultraviolet modes, we cut off the spectrum at a wave number k_p to a decaying power law with a specific index. Our results remain insensitive to the value of this cutoff wave number k_p, as demonstrated in appendix B. The initial spectra of $\delta\phi'$, $\mathbf{A}$, and $\mathbf{E}$ have been chosen correspondingly. The spectra of the electric part, $P_E(k)$ and of the magnetic part, $P_B(k)$ of the gauge field are defined via the comoving energy density,

$$\rho_g \equiv \frac{1}{2}\langle \mathbf{E}^2 + \mathbf{B}^2 \rangle = \int \frac{dk}{k} \left[P_E(k) + P_B(k) \right]. \tag{3.7}$$

3.2 Dynamics of axion and gauge fields: inferred from simulations

To study the dynamics of the axion-U(1) inflation model, we perform a series of simulations with different coupling strengths[7] $\alpha/f = 30$, 50, 65, 75, and 90. The parameters for these simulations are given in table 1. In figure 1, we present the evolution of different energy densities for $\alpha/f = 60$, 75, and 90. We show the evolution of the kinetic energy density, $\rho_{\rm kin}$ (dashed blue curves), potential energy density, $V(\phi)$ (solid cyan curves), and gauge field energy density, ρ_g (dot-dashed orange curves) in panels (a), (b), and (c) of figure 1 for the coupling strengths $\alpha/f = 60$, 75, and 90, respectively. Panels (d), (e), and (f) illustrate the evolution of ξ, while panels (g), (h), and (i) display the first slow-roll parameter, ϵ_H, for the corresponding cases. Inflation ends when $\epsilon_H = 1$. The vertical gray lines indicate the epoch of the end of inflation in each case. In this figure, e-folds N is defined[8] such that $N = 0$ marks the end of inflation in scenarios where the backreaction of the gauge fields on the axion dynamics is negligible. We denote the corresponding excess number of e-folds as ΔN_e.

For $\alpha/f = 60$, inflation ends when the potential and kinetic energies of the axion field become comparable and the backreaction of the gauge field becomes important post-inflation. The $\alpha/f = 30$ and 50 cases have the similar behavior. However, for $\alpha/f = 75$ and 90, the amplification of the gauge fields is significant to backreact on the evolution of the axion field

[7] It is to be noted that our coupling strengths are in the units of the inverse of the Planck mass. However, many previous studies use the inverse of the reduced Planck mass for normalization. To convert our coupling strengths to the reduced Planck mass normalization, our values need to be divided by $\sqrt{8\pi}$. table 1 provides the values of the coupling strengths in both units for clarity.

[8] As usual we define dimensionless e-folds N through the relation $dN = Hdt$ with cosmological time t and Hubble parameter H.

during inflation itself. When the backreaction of gauge fields on the axion field dynamics becomes significant during inflation, it reduces the axion field velocity, thereby extending the duration of inflation. The duration of inflation extends by $\Delta N_e = 1.7$ e-folds for $\alpha/f = 75$ and $\Delta N_e = 4.0$ e-folds for $\alpha/f = 90$ compared to cases with smaller coupling strengths. Our results are similar to those obtained in ref. [55], except that here the extended duration of inflation ΔN_e is slightly shorter.

In scenarios where the backreaction of gauge fields is negligible during inflation, it ends when the potential and kinetic energy become comparable. However, when gauge field backreaction is significant during inflation, it ends when the gauge field energy density is comparable to the axion potential energy.

3.3 Comparison with previous work in the homogeneous ϕ case

As discussed in the previous section, the backreaction of the gauge fields on the evolution of the axion field becomes significant during inflation for the coupling strengths; $\alpha/f = 75$ or 90. Previous semi-analytical studies have studied the evolution of this by ignoring spatial inhomogeneities [49, 51, 53, 57], and more recently, lattice simulations have been used to study this model [54, 55]. In ref. [51], backreaction is incorporated perturbatively, while the authors of ref. [53] use the gradient expansion formalism. In this section, we compare our results with these semi-analytical findings.

To compare our results with the previous semi-analytical studies, we neglect the axion field inhomogeneity in the evolution of the axion and gauge fields, i.e., equations (A.1), (A.8), and (A.9), and the contribution of the corresponding term in the total energy budget that governs the evolution of the background FLRW geometry, i.e., equation (A.6). We compare our results with previous semi-analytical works using a similar methodology to that in ref. [55]. In panels (d), (e), and (f) of figure 1, the cyan curves show the evolution of ξ, which governs the growth of the gauge fields. The purple curves in these panels represent the evolution of ξ when ϕ is assumed to be homogeneous, thus ignoring terms involving the spatial derivatives of ϕ in the evolution equations. The gray curve in panel (e) shows the predicted evolution of ξ from the semi-analytical GEF model used to study the axion-U(1) system described in refs. [49, 53]. From figure 1, we conclude that our simulation results align well with those of the GEF model. To have a good match with the GEF results, we note that the initial conditions for the simulation must be chosen so that the axion-U(1) system reaches the slow-roll regime a few e-folds before the gauge field backreaction becomes significant. This issue is discussed in detail in appendix C.

For the coupling strengths $\alpha/f = 75$ and 90, the spatial fluctuations of gauge fields become prominent and suppress the oscillatory features observed in the homogeneous case (purple curves in panels (e) and (f)). This attenuation has also been demonstrated in [55].

In figure 2, we show the spectra of the magnetic and electric components of the gauge fields for run D (blue curves) and run E (red curves). For run D, the spectra are shown from the initial time $N_i = -4.8$ to the final time $N_f = 1.2$, with intervals of $\Delta N = 0.5$. For run E, the spectra span from $N_i = -7$ to $N_f = 0$, which is also the time span shown in ref. [55]. We show the spectra of scalar field fluctuations at different times for these runs in appendix D.

As seen in figure 2, both magnetic and electric energy spectra initially peak at a scale close to the minimum wave number of the simulation box. As time progresses, the spectral peaks shift towards higher wave numbers, eventually reaching close to the maximum box wave number for run E. To extend the simulation to later times, a larger simulation box would be required.

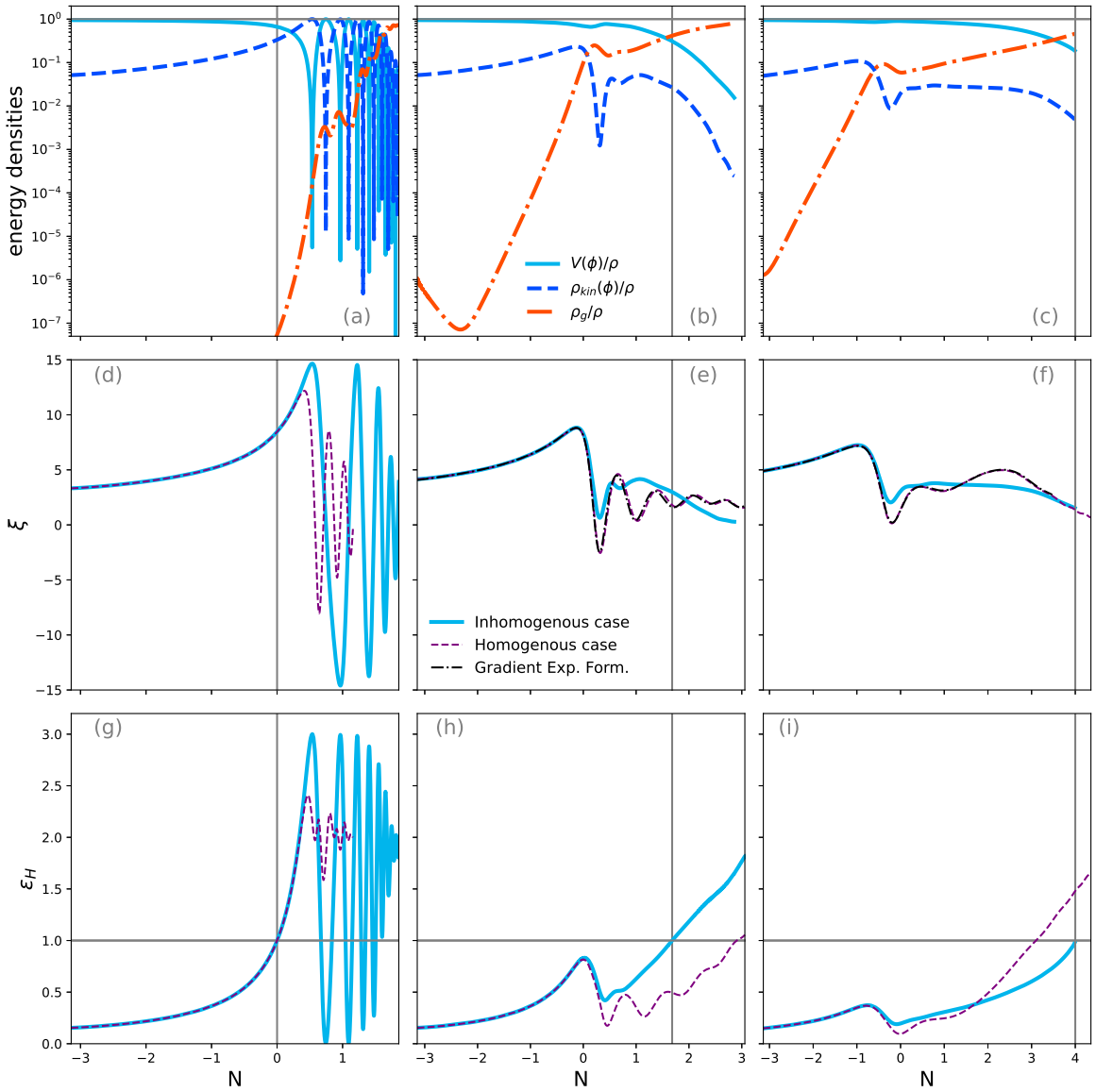

Figure 1: The time evolution of different energy densities (top row), ξ (middle row), and the first slow-roll parameter, ϵ_H (bottom row), is shown for $\alpha/f = 60$ (left column), 75 (middle column), and 90 (right column). The vertical gray lines indicate the end of inflation for each case. In the middle and bottom rows, the violet lines represent the time evolution of ξ and ϵ_H for the homogeneous ϕ case. In panels (e) and (f), the dot-dashed gray lines show the analytical GEF results discussed in refs. [47, 53].

4 Gravitational waves

In this section, we discuss the production of GWs during axion-U(1) inflation. The interaction between the axion and the gauge field results in the generation of GWs, as the produced gauge field has a nonzero transverse traceless component in its energy-momentum tensor. Additionally, scalar field spatial fluctuations produced by the gauge field also contribute to the generation of GWs. GWs are defined as the transverse traceless part of the tensor

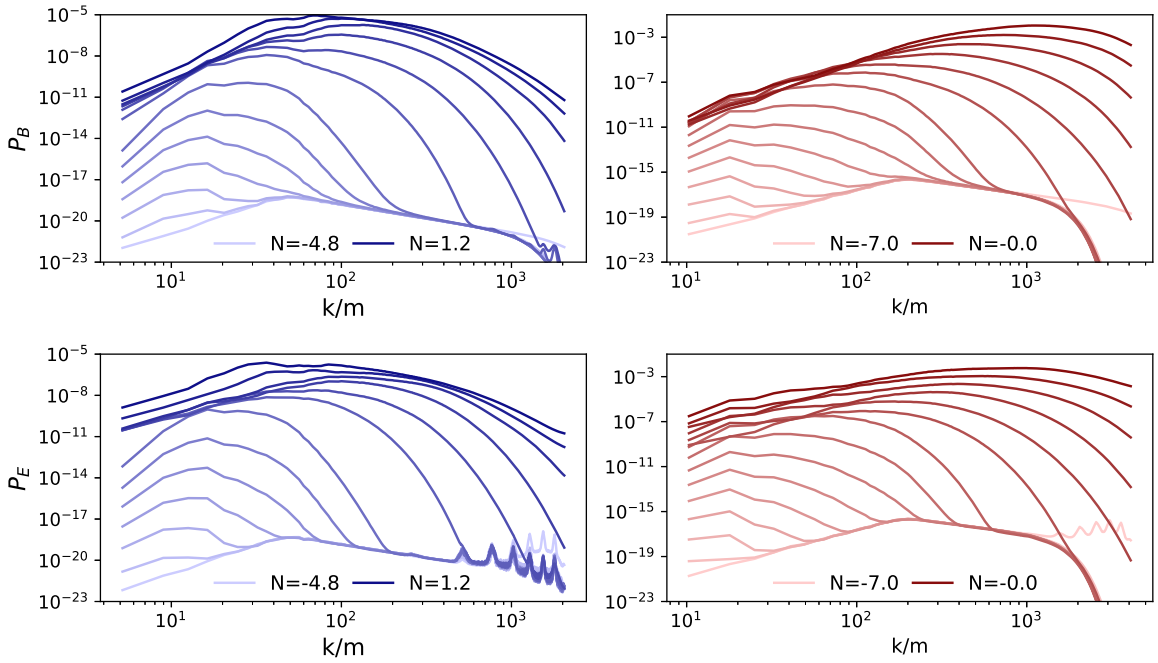

Figure 2: The spectra of the magnetic and electric components of the gauge field at different times are shown for $\alpha/f = 75$ (left, blue curves, run D) and $\alpha/f = 90$ (right, red curves, run E).

perturbations ($h_{ij}^{\rm TT}$) of the metric. Including these tensor perturbations, the metric is given by,

$$ds^2 = a^2\left(-d\eta^2 + (\delta_{ij} + h_{ij}^{\rm TT})dx^i dx^j\right) \tag{4.1}$$

The evolution of these tensor perturbations is governed by the Einstein equation. By linearizing the Einstein equation, we obtain;

$$\left(\frac{\partial^2}{\partial\eta^2} + k^2 - \frac{a''}{a}\right)\tilde{h}_{ij} = \frac{16\pi}{m_{\rm pl}^2}\frac{\tilde{T}_{ij}}{a}, \tag{4.2}$$

where, $\tilde{h}_{ij} = a h_{ij}^{\rm TT}$, $\tilde{T}_{ij} = a^2 T_{ij}^{\rm TT}$ and $T_{ij}^{\rm TT}$ denotes the transverse traceless part of the energy-momentum tensor (T_{ij}) of the source that led to the production of GWs. For the axion-U(1) model, the total T_{ij} is given by

$$T_{ij} = -B_i B_j - E_i E_j + a^2\partial_i\phi\partial_j\phi + ... \tag{4.3}$$

Here, the ellipsis represents the irrelevant terms proportional to g_{ij}. The energy density of the produced GWs is given by,

$$\rho_{\rm GW} \equiv \frac{1}{32\pi a^2}\langle h_{ij}^{\prime\rm TT} h_{ij}^{\prime\rm TT}\rangle = \frac{1}{32\pi a^4}\left(\langle\tilde{h}_{ij}'\tilde{h}_{ij}'\rangle - 2\mathcal{H}\langle\tilde{h}_{ij}\tilde{h}_{ij}'\rangle + \mathcal{H}^2\langle\tilde{h}_{ij}\tilde{h}_{ij}\rangle\right). \tag{4.4}$$

The density fraction of GWs at the present epoch is given by,

$$\Omega_{\rm GW}h^2 = \frac{\rho_{\rm GW}}{\rho_c}\Big|_0 = \frac{\rho_{\rm GW}}{\rho_r}\Big|_e \Omega_r h^2\,. \tag{4.5}$$

Here, $\Omega_r h^2$ represents the radiation density fraction at the present epoch and $\rho_{\rm GW}/\rho_r|_e$ denotes the ratio of the GW energy density to the total energy density at the time when the GW energy density reaches saturation.

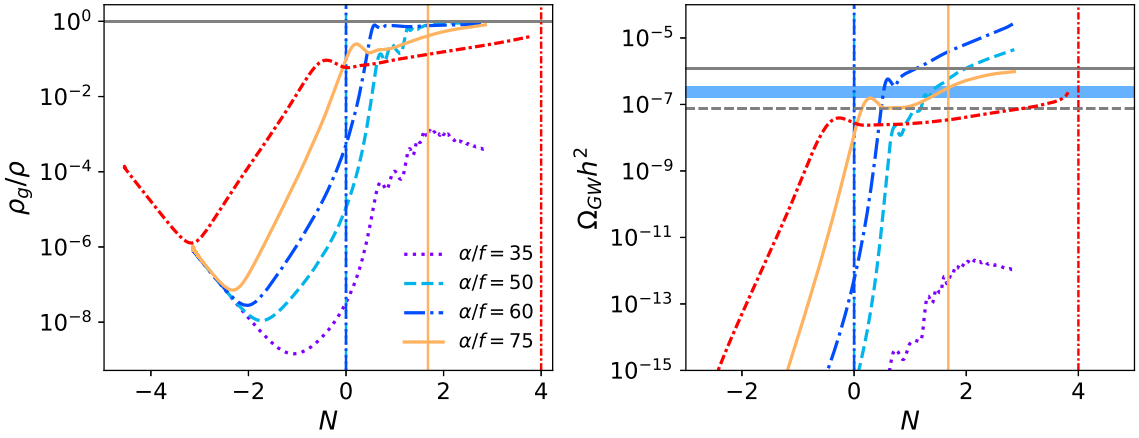

Figure 3: The time evolution of the gauge field energy density (left panel), normalized by the total energy density, and the density fraction of GWs (right panel) is shown for different values of α/f. The vertical lines indicate the end of inflation for each case. In the right panel, the horizontal solid gray line represents the bound on $\Omega_{\rm GW}h^2$ from Planck observations of the CMB, while the dashed gray line denotes the combined sensitivity of the future mission COrE and Euclid [69]. The blue band represents the CMB's S4 1σ and 2σ projections [70].

Further in this section, we study the production of GWs in the axion-gauge field scenario, considering both weak and strong coupling cases. The characteristic current frequency of these produced GWs is in GHz range and is determined by the horizon scale at the end of inflation, see equation (5.3). In figure 3, we show the time evolution of the gauge field energy density normalized by the total energy density in the left panel and the density fraction of the GWs in the right panel. The curves correspond to different coupling strengths; $\alpha/f = 30$ (dotted violet), 50 (dashed blue), 60 (dot-dashed blue), 75 (solid orange), and 90 (dot-dashed red). The vertical lines, in corresponding colors, represent the end of inflation for each case. The horizontal solid gray line indicates the bound on the GW energy density from the $\Delta N_{\rm eff}$ constraints from the CMB. The dashed gray curve represents the sensitivity of the future CMB-S4 mission. Our key findings regarding the constraints on the coupling strength between axion and gauge fields from the CMB bound on $\Delta N_{\rm eff}$ can be summarized as follows.

- As shown in figure 1, for $\alpha/f = 75$ and 90, once the energy density of the gauge field becomes comparable to the kinetic energy of the axion field, the velocity of the axion decreases. This reduction in axion velocity leads to a slower growth rate of the gauge field compared to the pre-backreaction stage. Consequently, the production rate of GWs also slows down, as shown in figure 3. The amplitude of the generated GWs remains below the bound obtained using Planck data for these cases up until the end of inflation.

- Previous studies [35, 36] indicated that the coupling strength above 70 leads to an overproduction of GWs, violating the $\Delta N_{\rm eff}$ bound from the Planck data of CMB.

This bound is for the case of chaotic potential, which is also considered for this case. However, we find that this bound is relaxed in the strong coupling case when gauge field backreaction becomes significant during inflation. The specific details of this bound depend on the duration of GW production after the end of inflation. As evident from figure 3, the produced GWs for $\alpha/f = 75$ may violate the bound from the Planck data on the GW amplitude, but this occurs 2–3 e-folds after the end of inflation. In our analysis, we have not considered the interaction of the gauge field with other standard model particles. For large coupling strengths, this interaction becomes important and may lead to instantaneous reheating, as discussed in section 4.2 of ref. [45]. Considering these effects would lead to the decay of the gauge field into other standard model species, further affecting GW production. If the gauge field energy density decays significantly within 2–3 e-folds after inflation, the produced GW amplitude will be smaller and may well be within the bound obtained from the Planck data (shown by the solid horizontal gray line in figure 3).

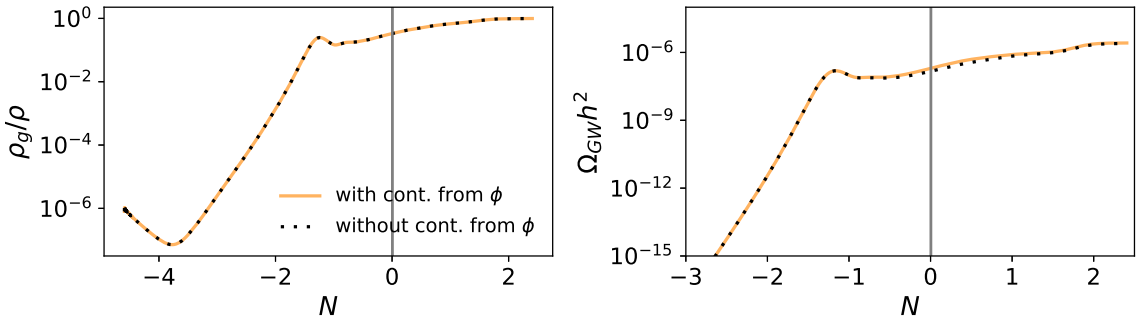

Figure 4: In this figure, we show the time evolution of ρ_g/ρ and $\Omega_{GW}h^2$ for $\alpha/f = 75$ for run D (solid yellow curves) and for a run (dotted black curves) analogous to run D in which the contribution of the ϕ term in the total energy-momentum tensor, given in equation(4.3), is neglected in the calculation of the GW energy density.

- Both axion and gauge fields contribute to GW production. To compare their contributions, we conduct a simulation analogous to run D, but with the axion field contribution neglected. We demonstrate this in figure 4. The left panel shows the time evolution of ρ_g/ρ, while the right panel is for $\Omega_{\rm GW}h^2$. The solid yellow curves correspond to the evolution for run D, whereas the dotted black curves represent a similar run where the contribution of the ϕ field was neglected in the estimation of the GW energy density. The vertical gray line marks the end of inflation for both runs. From this figure, we conclude that the contribution of the axion field to the GW energy can be neglected for most of the duration.

5 Magnetogenesis

There is indirect evidence of magnetic fields in the intergalactic medium, inferred from the non-detection of secondary GeV photons from blazars [71–74]. The presence of such intergalactic magnetic fields motivates the study of their generation in the early universe, potentially during inflation [75–85] or a first-order phase transition [86–90], for reviews see ref. [91–93]. In this section, we study the generation of magnetic fields within the axion-U(1)

inflation scenario and calculate their present day strength for different coupling strengths, α/f.

5.1 Gauge-field production

As discussed in section 3.2, the gauge fields are amplified due to the coupling between the axion and gauge fields. The produced gauge fields consist of two components; the magnetic part (hypermagnetic fields) and the electric part (hyperelectric fields). The energies in the electric component of the gauge fields will be converted into kinetic and magnetic energies [94] within one Hubble time after reheating due to the high conductivity of the universe post-reheating. By contrast, the hypermagnetic fields remain frozen because of the medium's high conductivity. However, this is not entirely accurate as hypermagnetic fields also decay as a power law due to their interaction with the charged plasma via the Lorentz force [92, 95–98], which we discuss later in this section. At the electroweak phase transition, these hypermagnetic fields will convert to standard magnetic fields, with their strength related to the hypermagnetic fields by the Weinberg angle, which is $\mathcal{O}(1)$. If strong enough, these magnetic fields could explain the presence of intergalactic magnetic fields in the present-day universe. We discuss this later in this section. The possibility of magnetogenesis in axion inflation has been studied in ref. [45] for coupling strengths $\alpha/f = 60$ and below. In this study, we also calculate the magnetic field strengths for larger coupling strengths; $\alpha/f = 75$ and 90 [55] in addition to the cases considered in [45].

First, we study the evolution of the electric and magnetic components of the gauge fields during inflation in our simulations. The root mean square value of the hypermagnetic field and its coherence length are given by,

$$B_{\rm rms} = \frac{1}{a^2}\sqrt{\int d\log k \cdot P_B(k)}\ , \qquad \text{and} \qquad L_c = \frac{\int d\log k \cdot k^{-1} \cdot P_B}{\int d\log k \cdot P_B}\ . \tag{5.1}$$

Similar definitions are used for the electric part of the gauge fields. Furthermore, assuming the universe evolves in a radiation-dominated phase from the end of our simulations, we can calculate the magnetic field strength today using the following expression:

$$B_{\rm rms}\big|_0 = 4.2\,\mu{\rm G}\sqrt{\frac{\int d\log k \cdot P_B}{\rho}}\ \sqrt{\frac{g_0}{3.36}}\left(\frac{B_{\rm CMB}}{3.3\ \mu{\rm G}}\right)\ . \tag{5.2}$$

Here, ρ represents the total energy density of the universe at the end of our simulations, g_0 represents the total number of relativistic degrees of freedom of the energy density today, and $B_{\rm CMB}$ is the magnetic field strength corresponding to the CMB energy density.

In figure 5, we demonstrate the evolution of the electric component with solid lines and the magnetic component with dashed lines for coupling strengths $\alpha/f = 30$ (green curve), 50 (red curve), 60 (orange curve), 75 (blue curve), and 90 (yellow curve). In the right panel, we illustrate the evolution of the coherence length for each coupling strength. The coherence length scale is normalized by the length scale corresponding to the Hubble horizon. The length scale corresponding to the Hubble horizon at the end of inflation is given by

$$L_H = \frac{a_0}{a_e}\frac{1}{H} = 1.97\times 10^{-17}{\rm pc}\left(\frac{10^{-6}m_{\rm pl}}{H}\right)^{1/2}\ . \tag{5.3}$$

In the above expression, we assume that the universe evolves adiabatically after inflation,

$$\frac{a_e}{a_0} = \left(\frac{g_{0s}}{g_{rs}}\right)^{1/3} \frac{T_0}{T_r} = 2.66 \times 10^{-29} \left(\frac{g_{0s}}{3.94} \frac{106.75}{g_{rs}}\right)^{1/3} \left(\frac{106.75}{g_r}\right)^{1/4} \frac{T_0}{2.73\text{K}} \left(\frac{10^{-6} m_{\rm pl}}{H}\right)^{1/2}, \tag{5.4}$$

where g_{rs} and g_{0s} denote the effective degrees of freedom in the entropy density at the end of inflation and the present epoch, respectively. We estimate the reheating temperature, T_r, by assuming instantaneous reheating using $3H^2 m_{\rm pl}^2 = (\pi^2/30) g_r T_r^4$.

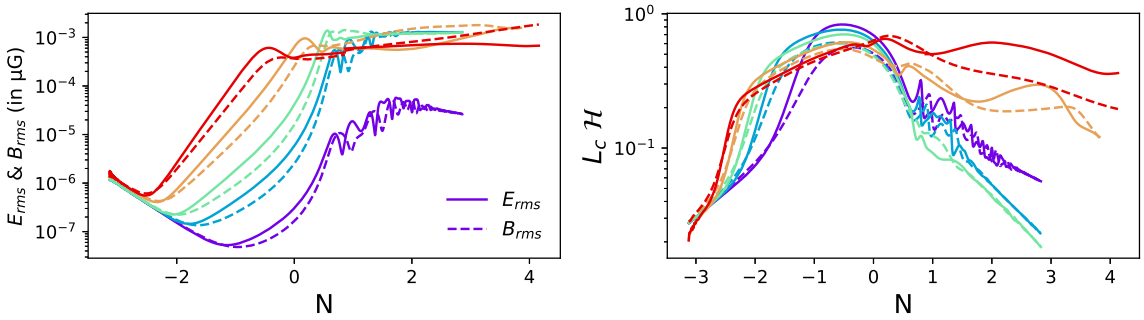

Figure 5: The evolution of the electric and magnetic components of the gauge field (left panel) and their coherence lengths (right panel) is shown for different values of α/f. The coherence lengths are normalized by the length scale corresponding to the Hubble horizon.

5.2 Evolution of gauge fields post inflation

After the end of inflation, the universe is dominated by the gauge field in the strong coupling regime of axion-U(1) system. Due to the dominance of the gauge field in the total energy budget, the effective equation of state resembles that of radiation dominance. We assume that reheating in this model occurs through the interaction of the gauge field with other Standard Model fields, as described in [45, 99]. Therefore, we can consider the universe as being radiation-dominated just after the end of inflation.

As discussed earlier, the gauge fields have a blue spectrum at the end of inflation and peaks at a scale smaller than the Hubble horizon size; see figure 5. We assume that the gauge fields remain unaffected from the end of inflation until the epoch when the universe's conductivity becomes much larger than the Hubble parameter. Once this epoch is reached, the electric component of the gauge field shortened out within a Hubble time scale, and the magnetic field becomes frozen into the rest of the plasma. After this epoch, the magnetic field interacts with the plasma via the Lorentz force and transfers some of its energy to the plasma. As a result, the magnetic field strength decreases. This nonlinear processing of the magnetic field begins when the Alfvén time becomes smaller than the Hubble time, which implies that the corresponding scale factor is $a_{\rm nl} \equiv a_H(\mathcal{H}\, L_c/V_A)$. Here, a_H corresponds to the scale factor at the horizon entry for a particular scale, and $V_A = \sqrt{B^2/(2(\rho+p)}$ is the Alfvén velocity.

In the nonlinear processing regime, the magnetic field strength decays as $(a_m/a_{nl})^{-1/3}$, and the coherence length (which corresponds to the peak scale in our case) increases as $(a_m/a_{nl})^{2/3}$ for the fully helical case. After incorporating the nonlinear processing of the

Run	α/f	$B_{\rm rms}\vert_0$ (G)	$L_c^{\rm NL}\vert_0$ (pc)	$B_{\rm bound}$ (G)	$B^1_{\rm rms}\vert_0$ (G)	$L_c^{1,{\rm NL}}\vert_0$ (pc)	$B^1_{\rm bound}$ (G)
A	35	6.2×10^{-17}	1.4×10^{-3}	8.4×10^{-14}	8.5×10^{-16}	7.1×10^{-3}	3.7×10^{-14}
B	50	4.6×10^{-16}	8.7×10^{-3}	3.4×10^{-14}	9.0×10^{-15}	9.9×10^{-2}	1.0×10^{-14}
C	60	1.7×10^{-15}	3.0×10^{-2}	1.8×10^{-14}	1.8×10^{-14}	9.9×10^{-2}	1.0×10^{-14}
D	75	1.2×10^{-14}	1.9×10^{-1}	7.2×10^{-15}	1.7×10^{-14}	1.5×10^{-1}	8.1×10^{-15}
E	90	1.4×10^{-14}	1.7×10^{-1}	7.6×10^{-15}	–	–	–

Table 2: $B_{\rm rms}\vert_0$ and $L_c^{\rm NL}\vert_0$ represent the present-day magnetic field strength and its coherence length obtained for each run, respectively. $B_{\rm bound}$ denotes the lower bound on the magnetic field strength based on blazar observations, where we assume $B_{\rm bound} = 10^{-17}{\rm G}\,(L/0.1{\rm Mpc})^{1/2}$.

fields, the magnetic field strength and its coherence length at the present epoch is given by,

$$B_{\rm rms}\big|_0 = 2.03\times10^{-14}\ {\rm G}\ \sqrt{\frac{\int d\log k\cdot P_B}{\rho}}\ \sqrt{\frac{g_0}{3.36}}\left(\frac{B_{\rm CMB}}{3.3\ \mu{\rm G}}\right) r^{1/3}\,, \tag{5.5}$$

and

$$L_c^{\rm NL} = 0.8\ {\rm pc}\ (\mathcal{H}L_c)\left(\frac{10^{-6}m_{\rm pl}}{H}\right)^{1/2} r^{-2/3}. \tag{5.6}$$

Here $r = \max(1, \mathcal{H}\ L_c/V_A)$ and $B_{\rm CMB}$ denotes the magnetic field strength corresponding to the CMB energy density. We show the time evolution of $\mathcal{H}L_c/V_A$ in appendix E for the runs given in table 1. After using the above expressions, we obtained the magnetic field strength and its coherence length corresponding to each coupling strength and the values are given in table 2. For the values given in columns 2 and 3 of table 2, we use $(\int d\log k\cdot P_B/\rho)^{1/2}$ and $\mathcal{H}L_c$ at the end of inflation in equation (5.5) and equation (5.6), respectively. However, for the values given in columns 4 and 5, we use the value of $(\int d\log k\cdot P_B/\rho)^{1/2}$ and $\mathcal{H}L_c$ one e-fold after inflation. In table 1, $B_{\rm bound}$ denotes the lower bound of magnetic field strength obtained from the blazars observation. Here we assume $B_{\rm bound} = 10^{-17}{\rm G}\,(L_C^{\rm NL}/0.1{\rm Mpc})^{1/2}$. From the values given in the table 2, we conclude that the magnetic field strength obtained in the axion-U(1) inflation model for coupling strengths $\alpha/f \geq 60$ can explain the required field strength to account for the non-observation of GeV photons in blazar observations. Recently, it has been suggested that the reconnection time, rather than the Alfvén time, is the relevant timescale for the decay of the nonlinear evolution of magnetic fields in the early universe [100–103]. In ref. [104], it was found that this makes the timescale approximately 50 times longer than the Alfvén time. If we account for this in our calculations, the length scale would decrease by a factor of $50^{2/3}$, and the magnetic field strength would increase by a factor of $50^{1/3}$ compared to the values mentioned in table 2. (If the decay is controlled by reconnection and the decay time still proportional to the square root of the conductivity, the exponents might be 4/7 and 2/7, respectively; see ref. [105].)

In our study, we have not considered the production of fermions resulting from interactions between gauge fields and fermions e.g., via the Schwinger effect. This has been discussed in refs. [49, 63] for the case of a homogeneous axion field. Based on [49], it can be inferred that the strength of the produced magnetic fields would decrease approximately by

a factor less than 10 (as can be seen from figures 6 and 7 in ref. [49]) upon incorporating the effects of charged currents generated by the Schwinger effect, although the exact reduction factor depends on the coupling strength. However, the impact of this effect in the case of an inhomogeneous axion field is not known, and we plan to address this in future work. In summary, we note that the gauge field strengths presented in table 2 could be reduced if the effect of the produced charged currents were included.

6 Curvature perturbations and its probability distribution function

In the previous analytical study [37–39], the formation of the PBHs from the large spatial fluctuations of the axion field generated by the backreaction of the gauge field on the axion dynamics has been studied. To estimate the abundance of PBHs, the authors used the Press-Schechter approach [106–108]. For this, one needs to know the probability distribution function (PDF) of the curvature perturbation variable, $\zeta = -H\delta\phi/\dot{\bar{\phi}}$. The PDF of ζ will be the same as the PDF of spatial fluctuations, $\delta\phi$, of the axion field. In these studies, this PDF has been assumed to be a χ^2-distribution due to the quadratic nature of the backreaction term of the gauge field in the scalar field dynamics. Using this, the authors in [37, 38] examined the constraints on α/f by using the constraints on PBHs abundances from BBN and CMB and obtained an upper bound on α/f. The obtained values of the upper bound are $\alpha/f \leq 115$ from [37] and $\alpha/f \leq 130$ from [38]. The obtained upper bound on α/f in these studies is such that this setup of axion-U(1) inflation is in the strong backreaction regime. Here we test this assumption and study the PDF of the axion field fluctuations in our simulations.

To study the evolution of the PDF of the axion field's spatial fluctuations, we use 3D snapshots from our simulations. At the beginning of our simulations, these fluctuations follow a Gaussian random field as set by the initial conditions. We normalize by the root mean square of the fluctuations in the axion field, σ_ϕ, and plot the PDF of $\delta\phi/\sigma_\phi \equiv (\phi - \bar{\phi})/\sigma_\phi$. Initially, it follows a standard normal distribution. In figure 6, we present the evolution of the PDFs for three different coupling strengths, $\alpha/f = 35$ (top panel), $\alpha/f = 60$ (mid panel) and $\alpha/f = 75$ (bottom panel). As evident from the top panel of figure 6, the PDF of $\delta\phi/\sigma_\phi$ is initially Gaussian and evolves into a χ^2-distribution with three degrees of freedom. However, in the case of strong coupling strength, the PDF starts as a Gaussian, transitions to a χ^2 distribution at an intermediate time, and reverts to a distribution closer to Gaussian at later times.

In a previous numerical study of axion-U(1) inflation [54], the authors investigated the PDF of curvature perturbations for $\alpha/f = 125$. However, due to the limited box size, their simulations covered only 6 e-folds during inflation and did not extend until the end of inflation. Extending the simulation until the end would require a significantly larger simulation box. In their study, the authors also observed that the PDF tends toward a Gaussian distribution. We would like to emphasize, however, that this result is not exclusive to cases where the gauge field backreaction is significant during inflation. As demonstrated in the middle panel of figure 6, the PDF of axion fluctuations for $\alpha/f = 60$ shows that this transition toward a Gaussian distribution also occurs when the backreaction becomes important after inflation.

Considering a distribution that is less non-Gaussian than the χ^2-distribution will result in a smaller PBH abundance[9]. This will relax the constraints on α/f. We will present a detailed study of the PBHs constraints in a future study.

[9]To accurately estimate PBH abundances, it is necessary to know the PDF of the smoothed curvature

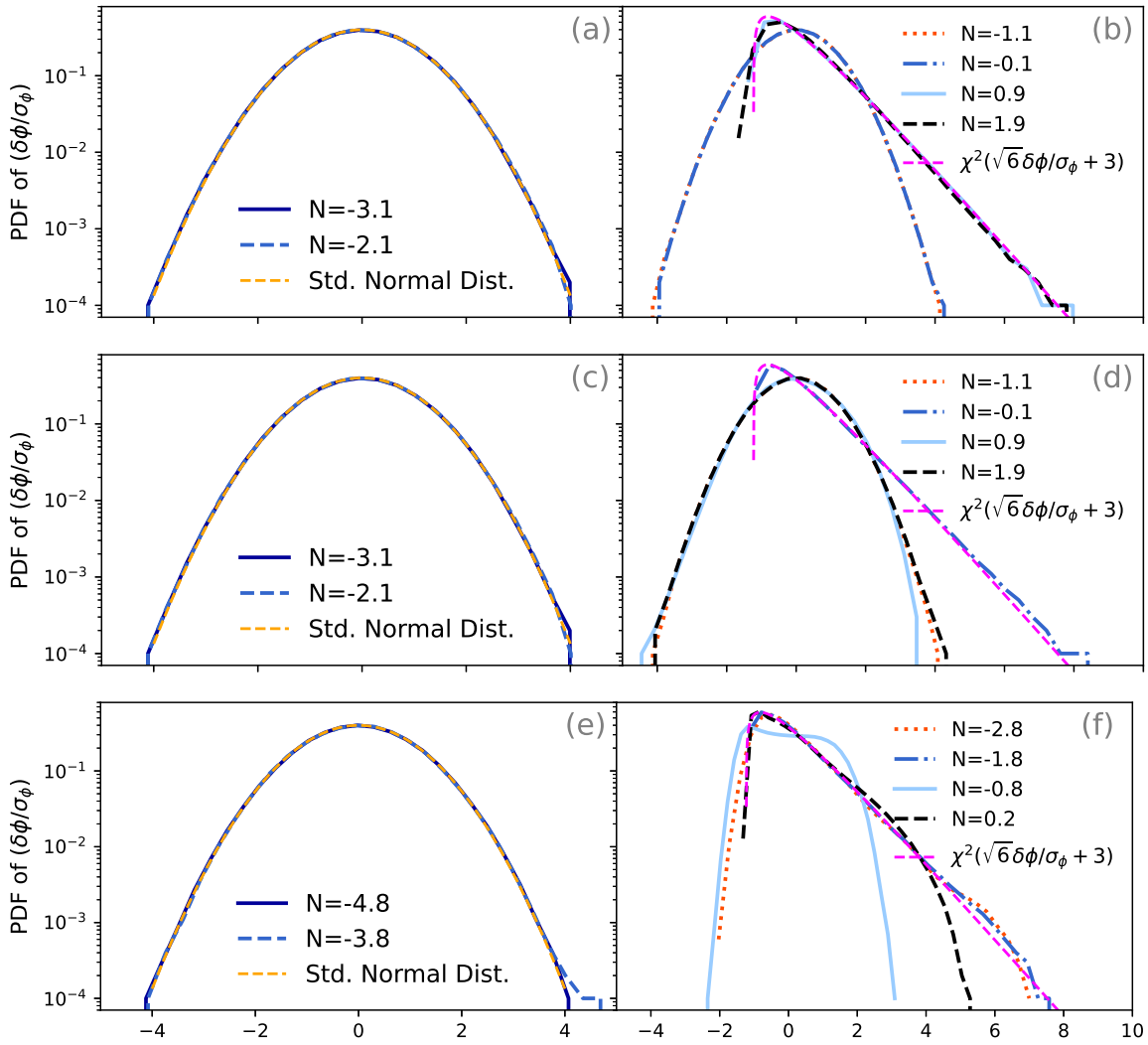

Figure 6: The PDFs of $\delta\phi/\sigma_\phi$ at different times for $\alpha/f = 35$ (top row), $\alpha/f = 60$ (middle row), and $\alpha/f = 75$ (bottom row). The yellow line represents the PDF for a Gaussian random field, while the magenta line shows the χ^2-distribution with three degrees of freedom for the variable $\sqrt{6}\delta\phi/\sigma_\phi + 3$. Here N represents the number of e-folds and $N = 0$ marks the end of inflation. In the bottom row, the initial time corresponds to $N = -4.8$, i.e., 1.7 e-folds less than that of the top and middle rows to address the prolonged duration of inflation by 1.7 e-folds for the case of $\alpha/f = 75$. In the left column, we show the PDFs at the earlier times of the simulation, while the right column displays them at the later stages.

7 Discussion and conclusion

In this paper, we study the axion-U(1) inflation model by simulating the dynamics of both the axion and the gauge fields. Our focus is on the regime where the gauge field backreaction

perturbations [37, 38]. Since the PDF of the smoothed curvature perturbations will be similar to, or even less non-Gaussian than, that of the unsmoothed perturbations, the constraints derived from the smoothed perturbations will be comparable to or less stringent than those from the unsmoothed perturbations.

on axion evolution becomes significant during inflation. Previous studies have addressed this scenario semi-analytically using perturbative [51, 57] and gradient expansion approaches [49, 53], which neglect axion field inhomogeneity. However, recent numerical simulations have incorporated these inhomogeneities [54–56]. For our study, we developed two new modules in the Pencil Code. Our numerical simulation results align well with previous semi-analytical studies for the homogeneous axion case and with recent numerical simulations for the inhomogeneous axion case.

We have analyzed the production of GWs and the PDF of spatial fluctuations in the axion field for $\alpha/f = 75$ and 90 in the Planck units. We also compare these results with cases of smaller coupling strengths ($\alpha/f = 35$, 50, and 60), where the gauge field backreaction is not significant during inflation. For $\alpha/f = 75$ and 90, the gauge field energy density becomes comparable to the potential energy of the axion field at the end of inflation and soon dominates the total energy budget of the universe. The produced GWs are within the bounds set by Planck data of CMB if only those produced until the end of inflation with no further production are considered. However, these GWs might exceed the bound if we account for those produced 2–3 e-folds during reheating after inflation and neglect the effects of the produced charged particles from the gauge fields.

In this study, we have neglected the interaction of the gauge field with other Standard Model particles. In cases of large coupling, such as $\alpha/f = 75$ and 90, the gauge field energy density is sufficient to provide instantaneous reheating, as the interaction rate of the gauge field with other particles is much larger than the Hubble expansion rate. This is discussed in detail in ref. [45]. Additionally, the produced large gauge fields may lead to the production of charged particles via the Schwinger effect [47, 63, 109–114]. Once the backreaction of these charged particles becomes significant, they may halt any further production of the gauge fields. Consequently, the produced GW energy density will saturate at a stage when these interactions become important. As these interactions may not be neglected until 23 e-folds after inflation, the bound from the Planck data may not be exceeded as a result. A detailed study incorporating the effects of other interactions will be conducted in future work.

The large-scale gauge fields produced in this model offer a possible explanation for intergalactic magnetic fields. We have explored this for small to large coupling strengths, α/f, and find that the resulting magnetic fields are above the lower bound on intergalactic magnetic fields inferred from blazar observations [71] for $\alpha/f \geq 60$. For the coupling strength $\alpha/f = 75$, the resulting magnetic field strength is $1.2 \times 10^{-14}\,\mathrm{G}$ with a coherence length of 0.19 pc. The lower bound on the magnetic field strength from blazar observations for this coherence length is $7.2 \times 10^{-15}\,\mathrm{G}$, based on the relation $B_{\rm bound} = 10^{-17}\,\mathrm{G}\,(L/0.1\,\mathrm{Mpc})^{1/2}$, as discussed in section 5.2. We note that the generated magnetic field strengths could be reduced upon incorporating the effects of charged currents produced through interactions between gauge fields and fermions, e.g., via the Schwinger effect. We leave a detailed investigation of this effect for future work.

Furthermore, we examine the PDF of the produced axion fluctuations. Understanding this PDF is crucial for studying the formation of PBHs in this model. Previous analytical studies considered it to be a χ^2-distribution with one or two degrees of freedom. In our study, we initialize axion fluctuations as a Gaussian random field. We find that the spatial fluctuations indeed transition to a χ^2-distribution at later times, but with three degrees of freedom. However, as the backreaction of the gauge field becomes significant, the system starts to resemble a Gaussian distribution. Incorporating this information in studies constraining the axion-gauge coupling from PBH abundance bounds will relax the existing constraints on this

coupling strength.

In this study, we examine the unsmoothed axion fluctuation distribution. However, to make accurate estimates, one needs to understand the distribution of the smoothed fluctuations. We believe that the distribution of smoothed fluctuations will be even closer to a Gaussian distribution compared to the unsmoothed case. We will provide a detailed study on this in a future work.

Acknowledgments

We would like to thank Angelo Caravano, Valerie Domcke, Yutong He, Oksana Iarygina, and Alberto Roper Pol for the discussions on this project. We are also indebted to Kai Schmitz and Oleksandr Sobol for providing the datasets used to compare with the results from the gradient expansion formalism for the homogeneous axion case as well as for the discussions on this comparison. R.S. and A.V. were supported by the Czech Science Foundation (GAČR), project 24-13079S. A.B. acknowledges funding from the Swedish Research Council (Vetenskapsrådet) under grant No. 2019-04234 and the National Science Foundation under Grant No. AST-2307698, and the NASA ATP Award 80NSSC22K0825. We also thank the Swedish National Allocations Committee for providing computing resources at the Center for Parallel Computers at the Royal Institute of Technology in Stockholm and the National Supercomputer Centre (NSC) in Linköping. Some simulations in this work were performed on the "Phoebe" computer cluster at CEICO/FZU. R.S. is grateful to Josef Dvořáček for assistance with setting up the Pencil Code on Phoebe. K.S. was partially supported by the Alexander Von Humboldt Foundation through the Carl Friedrich von Siemens Research Award. He thanks Volker Springel his host, as well as Torsten Ensslin and Eichiro Komatsu for warm hospitality during his stay at the Max-Planck Institute for Astrophysics, Garching.

Data availability. The source code used for the numerical solutions of this study, the Pencil Code, along with the module `special/backreact_infl` used in the present study, are freely available at https://github.com/pencil-code/pencil-code/. The numerical data and input files are available on http://norlx65.nordita.org/~brandenb/projects/axion-U1/.

A Implementation in the Pencil Code

As discussed in section 2, we use the Pencil Code for our simulations. To simulate the axion-U(1) inflation, we use the special modules `backreact_inf.f90` and `disp_current.f90`. The ϕ and FLRW background equations are solved in the 'backreact_infl.f90' module, while the **E** and **A** equations are solved in the 'disp_current.f90' module. By default, we use the Weyl gauge, but the Lorenz gauge can also be used by setting the `llongitudinalE` logical to false and the `llorenz_gauge_disp` logical to true. The governing equations in both Lorenz and Weyl gauges are described in the section A.1 and section A.2, respectively. In addition to the **E** and **A** variables, we also solve for A_0 in the Lorenz gauge. Additionally, we also solve for the production of gravitational waves using the equations in the gravitational module `gravitational_waves_hTXk.f90`; see ref. [115] for details. The Pencil Code employs a sixth-order finite difference method for spatial derivatives and a third-order Runge-Kutta method for time stepping.

A.1 Lorenz Gauge

In the Lorenz gauge, where $A_0' = \boldsymbol{\nabla} \cdot \mathbf{A}$, the system of equations (2.2), (2.4), (2.3) and (2.5) reduces to

$$\phi'' + 2\mathcal{H}\phi' - \nabla^2\phi + a^2\frac{\partial V}{\partial \phi} = \frac{\alpha}{f}a^{-2}\,\mathbf{E}\cdot\mathbf{B} \tag{A.1}$$

$$A_0' = \nabla\cdot\mathbf{A} \quad \text{(Lorenz gauge)} \tag{A.2}$$

$$A_0'' - \nabla^2 A_0 = \frac{\alpha}{f}\nabla\phi\cdot\mathbf{B} \quad \text{or} \quad (\nabla\cdot\mathbf{A})' - \nabla^2 A_0 = \frac{\alpha}{f}\nabla\phi\cdot\mathbf{B} \tag{A.3}$$

$$\mathbf{A}' = -\mathbf{E} + \nabla A_0 \tag{A.4}$$

$$\mathbf{E}' = \nabla\times\mathbf{B} - \frac{\alpha}{f}\left(\phi'\mathbf{B} + \nabla\phi\times\mathbf{E}\right). \tag{A.5}$$

$$\mathcal{H}^2 = \frac{8\pi}{3m_{\rm pl}^2}a^2\rho. \tag{A.6}$$

Here $\mathbf{E} = \nabla A_0 - \mathbf{A}'$ and $\mathbf{B} = \nabla\times\mathbf{A}$. In this case, we solve the equations (A.1), (A.2), (A.3), (A.4) and (A.5) for the axion-gauge field dynamics and equation (A.6) for the FLRW background evolution.

A.2 Weyl or temporal gauge

In the Weyl or temporal gauge, we have $A_0 = 0$ and instead of equations (A.2), (A.3), (A.4), and (A.5), we solve equations (A.7) and (A.8) and (A.9) for the gauge field evolution.

$$\mathbf{A}' = -\mathbf{E} \tag{A.7}$$

$$\mathbf{E}' = -\nabla^2\mathbf{A} + \nabla\Gamma - \frac{\alpha}{f}\left(\phi'\mathbf{B} + \nabla\phi\times\mathbf{E}\right) \tag{A.8}$$

$$\Gamma' = -(1-g_e^2)\nabla\cdot\mathbf{E} + g_e^2\frac{\alpha}{f}\nabla\phi\cdot\mathbf{B}. \tag{A.9}$$

Here $\Gamma = \nabla\cdot\mathbf{A}$. In appendix F, we present a comparison of the different gauges.

B Different initial cutoff wave numbers

As mentioned in section 3.1, we initialize the fluctuations of the axion and gauge fields using the Bunch-Davies initial condition. To neglect the contribution of large ultraviolet quantum fluctuation modes, we consider an initial power spectrum with a cutoff at a wave number k_p, above which the power spectrum follows a decaying power law. In this appendix, we demonstrate that the results of our simulations are independent of the initial value of k_p.

We conduct a simulation analogous to run D with $k_p/m = 94$ and $\alpha/f = 75$. The results are shown in figure 7, which depicts the evolution of ξ defined below equation (2.9) and the ratio of the gauge field energy density to the total energy density ρ_g/ρ for $k_p/m = 47$ (dot-dashed blue curves) and $k_p/m = 94$ (dashed violet curves). As evident from figure 7, both sets of curves overlap, indicating that the location of k_p does not affect the final results. The initial departure in the two curves in the right panel is because of the larger value of the initial amplitude of the gauge fields for the case $k_p/m = 94$. We also checked the dependence on the cutoff wave number for $\alpha/f = 90$ and came to similar conclusions for this case as well.

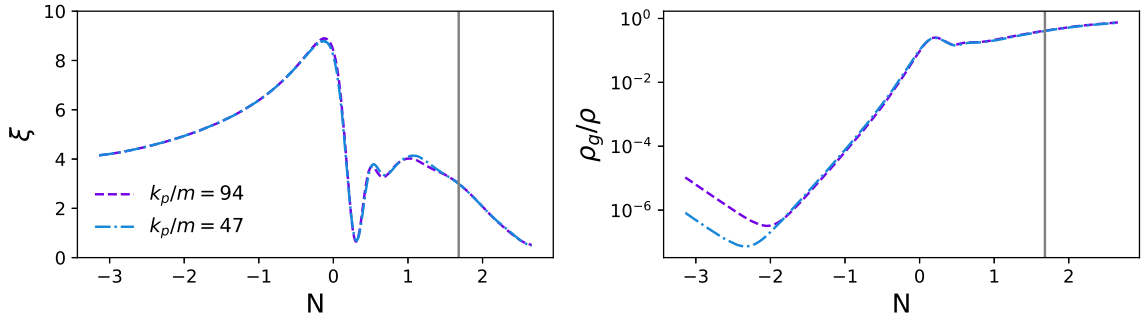

Figure 7: In this figure, we show the evolution of ξ and ρ_g/ρ for the runs D and its analogues run in which $k_p/m = 94$.

C Comparison with the GEF results

In section 3.3, we compared with the GEF results. Here, we discuss the need to choose initial conditions in the simulations that allow the system to relax into the slow-roll regime a few e-folds before the gauge field backreaction becomes significant. In our simulation, we initialize ϕ and ϕ' based on slow-roll conditions, starting the simulation 3.14 e-folds before the end of slow-roll inflation when gauge field backreaction is not yet significant. The spectra of **A** and **E** are initialized using the Bunch-Davies conditions. However, gauge modes closer to the horizon may already have been amplified, i.e., the Bunch-Davies conditions might not be an ideal initial condition for all gauge modes. We expect the system to naturally evolve to these solutions within a few e-folds, as can be seen for the coupling strength $\alpha/f = 75$ in figure 8, where this alignment occurs about one e-folds before the end of inflation, yielding a good match between GEF and our simulation results.

This is to be noted that, for $\alpha/f = 90$, we initialize the system at $N_i = -4.5$ to provide more time for it to approach the GEF results. If we instead initialize this case at $N_i = -3.14$, the gauge field energy density agrees with the GEF results only just before the gauge fields' backreaction becomes significant for the axion dynamics, as shown by the blue curve in figure 8. This initialization does not provide a good match for the evolution of ξ at later times, as shown in the bottom right panel in figure 8.

Importantly, the difference in gauge field energy density between GEF and our simulation remains small after the time of backreaction even in the case in which we initialize at $N_i = -3.14$ for $\alpha/f = 90$. Therefore, while choosing better initial conditions could improve consistency with GEF, it would not significantly impact the predictions for magnetic fields and gravitational waves.

D Spectrum of scalar field fluctuations

At the end of section 3.3, we compared with the results for runs D and E. Here, we provide the spectra of the scalar field fluctuation $P_{\delta\phi}$. The left- and right-hand panels of figure 9 show those spectra for runs D and E, respectively. The light to dark shades represent different times, with each curve separated by $\Delta N = 0.5$. They agree well with those of ref. [55].

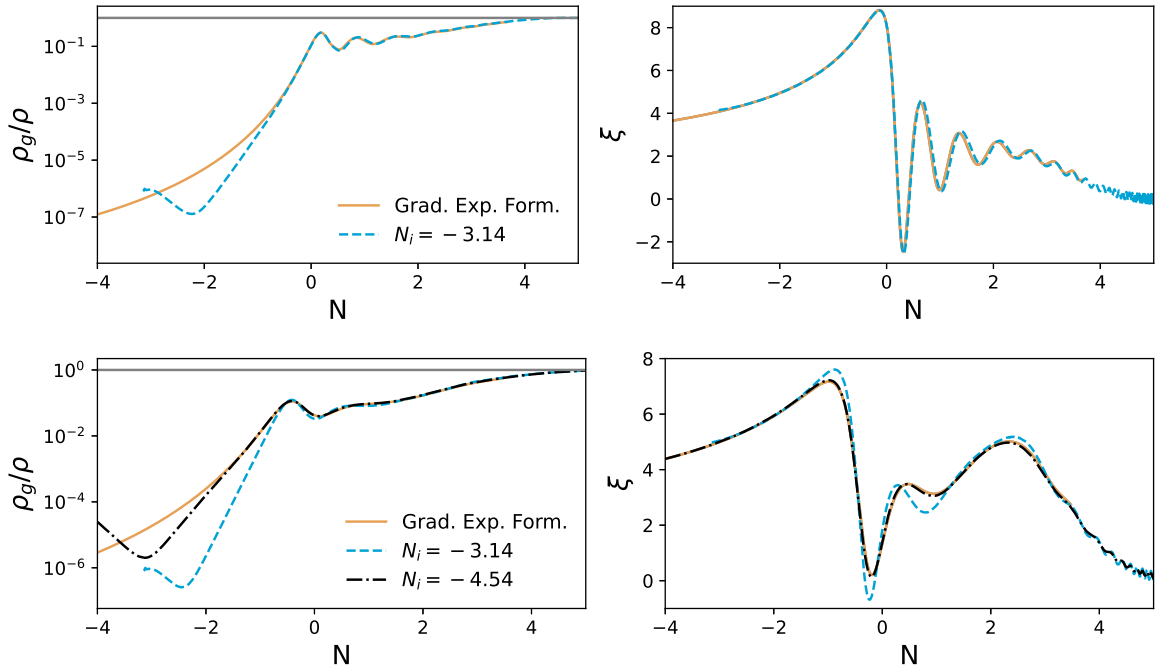

Figure 8: The evolution of the ratio of gauge field energy density to the total energy density (left panel) and the parameter ξ is shown in this figure. The yellow curves represent the results from the GEF approach, while the blue and black curves show results from our simulation for the homogeneous axion case. The black curve corresponds to the case where we start at $N_i = -4.54$ e-folds before the end of slow-roll inflation, and the blue curve is for $N_i = -3.14$. The upper and lower rows are for the coupling strength, $\alpha = 75$ and 90, respectively.

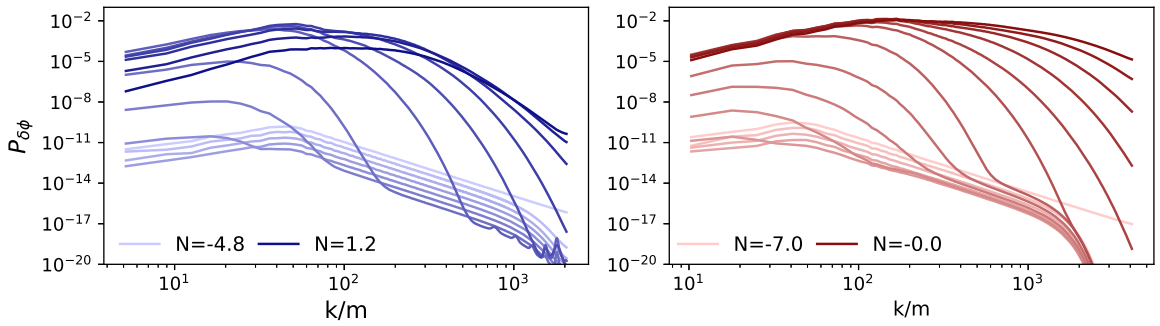

Figure 9: The spectrum of scalar field fluctuations is shown, with the left panel representing run D and the right panel representing run E. The curves progress in time from lighter to darker shades, each separated by $\Delta N = 0.5$.

E Time evolution of $\mathcal{H}\ L_c/V_A$

In section 5.2, we discussed that the nonlinear processing of the magnetic field depends on the ratio of the Alfvén time scale to the Hubble time scale, $\mathcal{H}\ L_c/V_A$. This ratio shown in figure 10 decides when the nonlinear processing of the magnetic field will begin in the plasma after its generation. The different curves show the time evolution of $\mathcal{H}\ L_c/V_A$ for different

values of α/f.

From this figure, we see that after the end of inflation, the value of $\mathcal{H}\ L_c/V_A$ is less than 1 for all cases except for $\alpha/f = 35$. Therefore, as discussed in section 5.2, we conclude that the magnetic fields are in the nonlinear processing regime at the end of inflation, except in the case of $\alpha/f = 35$.

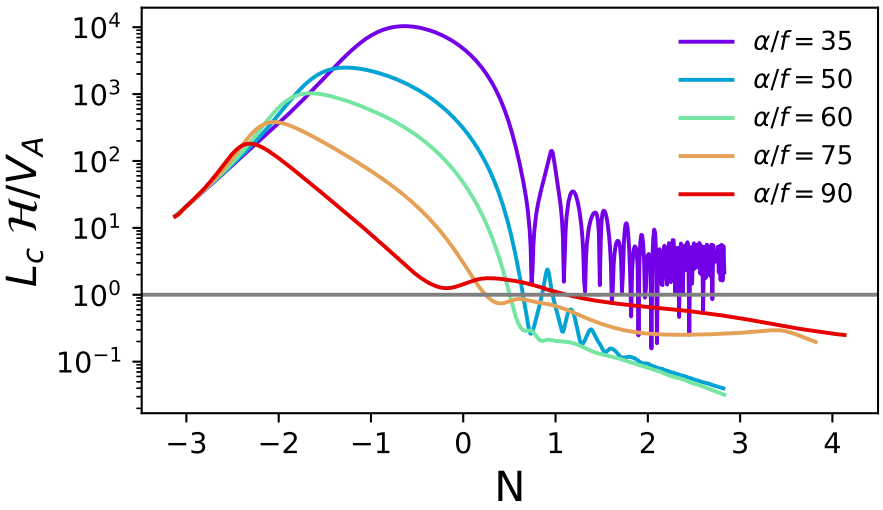

Figure 10: Time evolution of $\mathcal{H}\ L_c/V_A$ for the runs given in table 1.

F Additional tests

In appendix A, we stated that we use the Weyl gauge by default. Here, we compare with the Lorenz gauge and show that with both gauges, the constraint equation (2.4) is obeyed.

F.1 Weyl vs Lorenz gauge

We use the Weyl gauge to evolve the gauge field in the simulations discussed in this paper. However, the Lorenz gauge can also be used to solve these equations, although this requires solving an additional equationthe evolution of the temporal component, A_0. The Lorenz gauge has been used in previous studies [45, 54].

In this section, we compare the results of run D for the Weyl and Lorenz gauges. Thus, we run a simulation analogous to run D in the Lorenz gauge, using equation (A.1), and show the time evolution of the parameter ξ and the ratio ρ_g/ρ in figure 11. From this figure, it is clear that the evolution in the Lorenz gauge (dashed-dotted blue curves) closely matches that in the Weyl gauge (dashed violet curves). Thus, either gauge can be used for the numerical evolution of the gauge field equations.

F.2 Constraint equation check

As discussed in appendix A, with the Pencil Code, the axion-U(1) inflation model can be solved using either the Lorenz gauge or the Weyl gauge. While the simulations discussed in the main text use the Weyl gauge, we provide a comparison of the results obtained with both

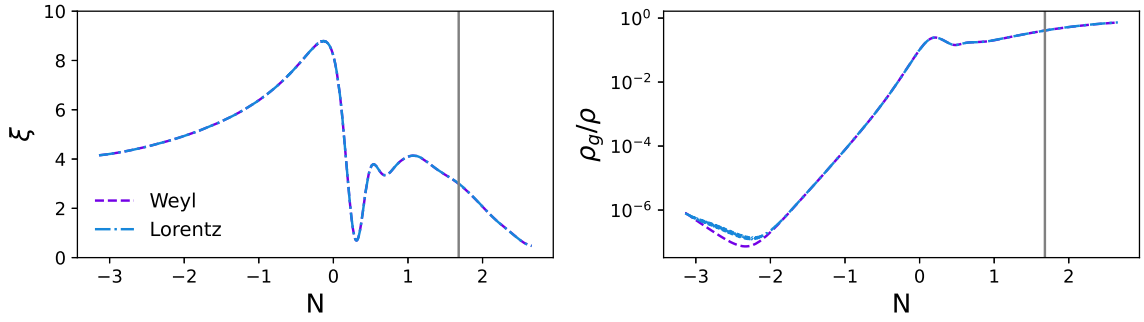

Figure 11: In this figure, we show the evolution of ξ and the ratio ρ_g/ρ for run D (dashed violet curves), along with its analogous run where the gauge field equation is evolved using the Lorenz gauge (dashed-dotted blue curves).

gauges in the appendix F.1. Here, we demonstrate the status of the constraint equation (2.4) with time in one of our simulations. To do this, we use the following expression

$$C.E. = \left\langle \frac{\nabla \cdot \mathbf{E} - \frac{\alpha}{f}\boldsymbol{\nabla}\phi \cdot \mathbf{B}}{\sqrt{(\nabla \cdot \mathbf{E})^2 + (\frac{\alpha}{f}\boldsymbol{\nabla}\phi \cdot \mathbf{B})^2}} \right\rangle. \tag{F.1}$$

In figure 12, the left panel shows the status of the constraint equation in the Weyl gauge,

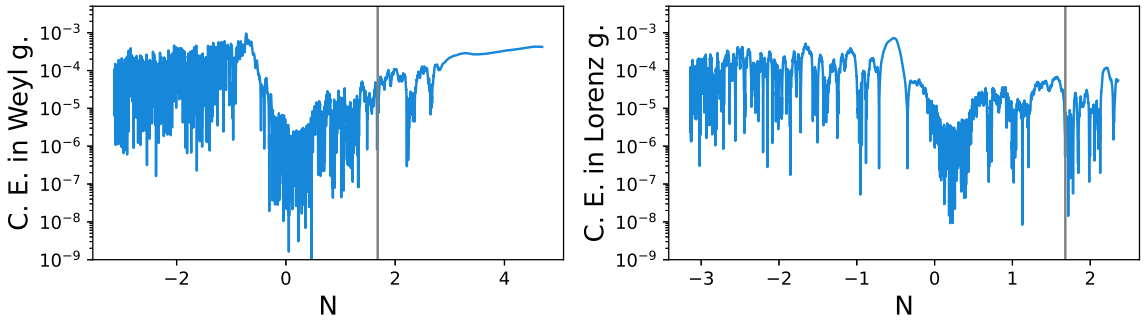

Figure 12: The status of the constraint equation (2.4) with time in Weyl (left panel) and Lorenz gauge (right panel) is shown for the run D.

while the right panel shows the gauge condition in the Lorenz gauge. Both panels correspond to run D. Additionally, we also check the accuracy with which the constraint equation is satisfied for different values of g_e^2 defined in equation (A.9). We find that for $g_e^2 = 2$, 1, or 0, the accuracy remains at similar levels shown in figure 12.

References

[1] A. Starobinsky, *A new type of isotropic cosmological models without singularity*, *Phys. Lett. B* **91** (1980) 99.

[2] A. H. Guth, *Inflationary universe: A possible solution to the horizon and flatness problems*, *Phys. Rev. D* **23** (1981) 347.

[3] A. Linde, *A new inflationary universe scenario: A possible solution of the horizon, flatness, homogeneity, isotropy and primordial monopole problems*, *Phys. Lett. B* **108** (1982) 389.

[4] A. Albrecht and P. J. Steinhardt, *Cosmology for grand unified theories with radiatively induced symmetry breaking*, *Phys. Rev. Lett.* **48** (1982) 1220.

[5] D. Kazanas, *Dynamics of the universe and spontaneous symmetry breaking*, *Astrophys. J. Lett.* **241** (1980) L59.

[6] K. Sato, *The first order phase transition of a vacuum and baryon-number domain structure of the universe*, *Prog. Part. Nucl. Phys.* **6** (1981) 311.

[7] V. F. Mukhanov and G. V. Chibisov, *Quantum Fluctuations and a Nonsingular Universe*, *JETP Lett.* **33** (1981) 532.

[8] G. V. Chibisov and V. F. Mukhanov, *Galaxy formation and phonons*, *Mon. Not. Roy. Astron. Soc.* **200** (1982) 535.

[9] V. Mukhanov, *Quantum Cosmological Perturbations: Predictions and Observations*, *Eur. Phys. J. C* **73** (2013) 2486 [1303.3925].

[10] A. A. Starobinsky, *Dynamics of Phase Transition in the New Inflationary Universe Scenario and Generation of Perturbations*, *Phys. Lett. B* **117** (1982) 175.

[11] A. H. Guth and S. Y. Pi, *Fluctuations in the New Inflationary Universe*, *Phys. Rev. Lett.* **49** (1982) 1110.

[12] S. Hawking, *The development of irregularities in a single bubble inflationary universe*, *Phys. Lett. B* **115** (1982) 295.

[13] J. M. Bardeen, P. J. Steinhardt and M. S. Turner, *Spontaneous Creation of Almost Scale - Free Density Perturbations in an Inflationary Universe*, *Phys. Rev. D* **28** (1983) 679.

[14] Planck Collaboration, N. Aghanim et al., *Planck 2018 results. I. Overview and the cosmological legacy of Planck*, *Astron. Astrophys.* **641** (2020) A1 [1807.06205].

[15] D. Baumann, *Inflation*, in *Theoretical Advanced Study Institute in Elementary Particle Physics: Physics of the Large and the Small*, pp. 523–686, 2011, 0907.5424, DOI.

[16] L. Sriramkumar, *An introduction to inflation and cosmological perturbation theory*, *Curr. Sci.* **97** (2009) 868 [0904.4584].

[17] J. Martin, C. Ringeval and V. Vennin, *Encyclopædia Inflationaris*, *Phys. Dark Univ.* **5-6** (2014) 75 [1303.3787].

[18] Planck Collaboration, Y. Akrami et al., *Planck 2018 results. X. Constraints on inflation*, *Astron. Astrophys.* **641** (2020) A10 [1807.06211].

[19] D. Chowdhury, J. Martin, C. Ringeval and V. Vennin, *Assessing the scientific status of inflation after Planck*, *Phys. Rev. D* **100** (2019) 083537 [1902.03951].

[20] K. Freese, J. A. Frieman and A. V. Olinto, *Natural inflation with pseudo nambu-goldstone bosons*, *Phys. Rev. Lett.* **65** (1990) 3233.

[21] F. C. Adams, J. R. Bond, K. Freese, J. A. Frieman and A. V. Olinto, *Natural inflation: Particle physics models, power law spectra for large scale structure, and constraints from COBE*, *Phys. Rev. D* **47** (1993) 426 [hep-ph/9207245].

[22] L. McAllister, E. Silverstein and A. Westphal, *Gravity Waves and Linear Inflation from Axion Monodromy*, *Phys. Rev. D* **82** (2010) 046003 [0808.0706].

[23] N. Kaloper and L. Sorbo, *A Natural Framework for Chaotic Inflation*, *Phys. Rev. Lett.* **102** (2009) 121301 [0811.1989].

[24] J. E. Kim, H. P. Nilles and M. Peloso, *Completing natural inflation*, *JCAP* **01** (2005) 005 [hep-ph/0409138].

[25] M. M. Anber and L. Sorbo, *Naturally inflating on steep potentials through electromagnetic dissipation*, *Phys. Rev. D* **81** (2010) 043534 [0908.4089].

[26] P. Adshead and M. Wyman, *Chromo-Natural Inflation: Natural inflation on a steep potential with classical non-Abelian gauge fields*, *Phys. Rev. Lett.* **108** (2012) 261302 [1202.2366].

[27] A. Notari and K. Tywoniuk, *Dissipative Axial Inflation*, *JCAP* **12** (2016) 038 [1608.06223].

[28] R. Z. Ferreira and A. Notari, *Thermalized Axion Inflation*, *JCAP* **09** (2017) 007 [1706.00373].

[29] E. Pajer and M. Peloso, *A review of Axion Inflation in the era of Planck*, *Class. Quant. Grav.* **30** (2013) 214002 [1305.3557].

[30] L. Sorbo, *Parity violation in the Cosmic Microwave Background from a pseudoscalar inflaton*, *JCAP* **06** (2011) 003 [1101.1525].

[31] M. M. Anber and L. Sorbo, *Non-Gaussianities and chiral gravitational waves in natural steep inflation*, *Phys. Rev. D* **85** (2012) 123537 [1203.5849].

[32] P. Adshead, E. Martinec and M. Wyman, *Gauge fields and inflation: Chiral gravitational waves, fluctuations, and the Lyth bound*, *Phys. Rev. D* **88** (2013) 021302 [1301.2598].

[33] P. Adshead, J. T. Giblin and Z. J. Weiner, *Gravitational waves from gauge preheating*, *Phys. Rev. D* **98** (2018) 043525 [1805.04550].

[34] P. Adshead, L. Pearce, M. Peloso, M. A. Roberts and L. Sorbo, *Gravitational waves from fermion production during axion inflation*, *JCAP* **10** (2019) 018 [1904.10483].

[35] P. Adshead, J. T. Giblin, M. Pieroni and Z. J. Weiner, *Constraining Axion Inflation with Gravitational Waves across 29 Decades in Frequency*, *Phys. Rev. Lett.* **124** (2020) 171301 [1909.12843].

[36] P. Adshead, J. T. Giblin, M. Pieroni and Z. J. Weiner, *Constraining axion inflation with gravitational waves from preheating*, *Phys. Rev. D* **101** (2020) 083534 [1909.12842].

[37] A. Linde, S. Mooij and E. Pajer, *Gauge field production in supergravity inflation: Local non-gaussianity and primordial black holes*, *Phys. Rev. D* **87** (2013) 103506.

[38] E. Bugaev and P. Klimai, *Axion inflation with gauge field production and primordial black holes*, *Phys. Rev. D* **90** (2014) 103501 [1312.7435].

[39] V. Domcke, F. Muia, M. Pieroni and L. T. Witkowski, *PBH dark matter from axion inflation*, *JCAP* **07** (2017) 048 [1704.03464].

[40] V. Domcke, B. von Harling, E. Morgante and K. Mukaida, *Baryogenesis from axion inflation*, *JCAP* **10** (2019) 032 [1905.13318].

[41] V. Domcke, Y. Ema, K. Mukaida and M. Yamada, *Spontaneous Baryogenesis from Axions with Generic Couplings*, *JHEP* **08** (2020) 096 [2006.03148].

[42] W. D. Garretson, G. B. Field and S. M. Carroll, *Primordial magnetic fields from pseudoGoldstone bosons*, *Phys. Rev. D* **46** (1992) 5346 [hep-ph/9209238].

[43] M. M. Anber and L. Sorbo, *N-flationary magnetic fields*, *JCAP* **10** (2006) 018 [astro-ph/0606534].

[44] T. Fujita, R. Namba, Y. Tada, N. Takeda and H. Tashiro, *Consistent generation of magnetic fields in axion inflation models*, *JCAP* **05** (2015) 054 [1503.05802].

[45] P. Adshead, J. T. Giblin, T. R. Scully and E. I. Sfakianakis, *Magnetogenesis from axion inflation*, *JCAP* **10** (2016) 039 [1606.08474].

[46] M. Kamarpour and O. Sobol, *Magnetogenesis in Natural Inflation Model*, *Ukr. J. Phys.* **63** (2018) 673.

[47] O. O. Sobol, E. V. Gorbar and S. I. Vilchinskii, *Backreaction of electromagnetic fields and the Schwinger effect in pseudoscalar inflation magnetogenesis*, *Phys. Rev. D* **100** (2019) 063523 [1907.10443].

[48] E. V. Gorbar, K. Schmitz, O. O. Sobol and S. I. Vilchinskii, *Hypermagnetogenesis from axion inflation: Model-independent estimates*, *Phys. Rev. D* **105** (2022) 043530 [2111.04712].

[49] E. V. Gorbar, K. Schmitz, O. O. Sobol and S. I. Vilchinskii, *Gauge-field production during axion inflation in the gradient expansion formalism*, *Phys. Rev. D* **104** (2021) 123504 [2109.01651].

[50] S.-L. Cheng, W. Lee and K.-W. Ng, *Numerical study of pseudoscalar inflation with an axion-gauge field coupling*, *Phys. Rev. D* **93** (2016) 063510 [1508.00251].

[51] V. Domcke, V. Guidetti, Y. Welling and A. Westphal, *Resonant backreaction in axion inflation*, *JCAP* **09** (2020) 009 [2002.02952].

[52] M. Peloso and L. Sorbo, *Instability in axion inflation with strong backreaction from gauge modes*, *JCAP* **01** (2023) 038 [2209.08131].

[53] O. O. Sobol, A. V. Lysenko, E. V. Gorbar and S. I. Vilchinskii, *Gradient expansion formalism for magnetogenesis in the kinetic coupling model*, *Phys. Rev. D* **102** (2020) 123512 [2010.13587].

[54] A. Caravano, E. Komatsu, K. D. Lozanov and J. Weller, *Lattice simulations of axion-U(1) inflation*, *Phys. Rev. D* **108** (2023) 043504 [2204.12874].

[55] D. G. Figueroa, J. Lizarraga, A. Urio and J. Urrestilla, *Strong Backreaction Regime in Axion Inflation*, *Phys. Rev. Lett.* **131** (2023) 151003 [2303.17436].

[56] A. Caravano and M. Peloso, *Unveiling the nonlinear dynamics of a rolling axion during inflation*, 2407.13405.

[57] V. Domcke, Y. Ema and S. Sandner, *Perturbatively including inhomogeneities in axion inflation*, *JCAP* **03** (2024) 019 [2310.09186].

[58] M. Y. Khlopov, *Primordial Black Holes*, *Res. Astron. Astrophys.* **10** (2010) 495 [0801.0116].

[59] M. Sasaki, T. Suyama, T. Tanaka and S. Yokoyama, *Primordial black holes—perspectives in gravitational wave astronomy*, *Class. Quant. Grav.* **35** (2018) 063001 [1801.05235].

[60] A. Escrivà, F. Kuhnel and Y. Tada, *Primordial Black Holes*, 2211.05767.

[61] S. S. Mishra and V. Sahni, *Primordial Black Holes from a tiny bump/dip in the Inflaton potential*, *JCAP* **04** (2020) 007 [1911.00057].

[62] H. V. Ragavendra, P. Saha, L. Sriramkumar and J. Silk, *Primordial black holes and secondary gravitational waves from ultraslow roll and punctuated inflation*, *Phys. Rev. D* **103** (2021) 083510 [2008.12202].

[63] V. Domcke and K. Mukaida, *Gauge Field and Fermion Production during Axion Inflation*, *JCAP* **11** (2018) 020 [1806.08769].

[64] L. Leblond and E. Pajer, *Resonant Trispectrum and a Dozen More Primordial N-point functions*, *JCAP* **01** (2011) 035 [1010.4565].

[65] A. Caravano, *Simulating the inflationary Universe: from single-field to the axion-U(1) model*, Ph.D. thesis, Munich U., Munich U., 7, 2022. 2209.13616. 10.5282/edoc.30905.

[66] P. Adshead, J. T. Giblin, R. Grutkoski and Z. J. Weiner, *Gauge preheating with full general relativity*, *JCAP* **03** (2024) 017 [2311.01504].

[67] D. C. Galanti, P. Conzinu, G. Marozzi and S. Santos da Costa, *Gauge invariant quantum backreaction in U(1) axion inflation*, 2406.19960.

[68] Pencil Code Collaboration, A. Brandenburg, A. Johansen, P. Bourdin, W. Dobler, W. Lyra, M. Rheinhardt, S. Bingert, N. Haugen, A. Mee, F. Gent, N. Babkovskaia, C.-C. Yang, T. Heinemann, B. Dintrans, D. Mitra, S. Candelaresi, J. Warnecke, P. Käpylä, A. Schreiber, P. Chatterjee, M. Käpylä, X.-Y. Li, J. Krüger, J. Aarnes, G. Sarson, J. Oishi, J. Schober, R. Plasson, C. Sandin, E. Karchniwy, L. Rodrigues, A. Hubbard, G. Guerrero, A. Snodin, I. Losada, J. Pekkilä and C. Qian, *The Pencil Code, a modular MPI code for partial differential equations and particles: multipurpose and multiuser-maintained*, *J. Open Source Software* **6** (2021) 2807.

[69] L. Pagano, L. Salvati and A. Melchiorri, *New constraints on primordial gravitational waves from Planck 2015*, *Phys. Lett. B* **760** (2016) 823 [1508.02393].

[70] K. Abazajian et al., *CMB-S4 Science Case, Reference Design, and Project Plan*, 1907.04473.

[71] A. Neronov and I. Vovk, *Evidence for strong extragalactic magnetic fields from Fermi observations of TeV blazars*, *Science* **328** (2010) 73 [1006.3504].

[72] A. M. Taylor, I. Vovk and A. Neronov, *Extragalactic magnetic fields constraints from simultaneous GeV-TeV observations of blazars*, *Astron. Astrophys.* **529** (2011) A144 [1101.0932].

[73] Fermi-LAT Collaboration, J. Finke, L. Reyes and M. Georganopoulos, *Constraints on the Intergalactic Magnetic Field from Gamma-Ray Observations of Blazars*, *eConf* **C121028** (2012) 365 [1303.5093].

[74] J. D. Finke, L. C. Reyes, M. Georganopoulos, K. Reynolds, M. Ajello, S. J. Fegan and K. McCann, *Constraints on the Intergalactic Magnetic Field with Gamma-Ray Observations of Blazars*, *Astrophys. J.* **814** (2015) 20 [1510.02485].

[75] M. S. Turner and L. M. Widrow, *Inflation Produced, Large Scale Magnetic Fields*, *Phys. Rev. D* **37** (1988) 2743.

[76] B. Ratra, *Cosmological 'seed' magnetic field from inflation*, *Astrophys. J. Lett.* **391** (1992) L1.

[77] V. Demozzi, V. Mukhanov and H. Rubinstein, *Magnetic fields from inflation?*, *JCAP* **08** (2009) 025 [0907.1030].

[78] J. Martin and J. Yokoyama, *Generation of Large-Scale Magnetic Fields in Single-Field Inflation*, *JCAP* **01** (2008) 025 [0711.4307].

[79] R. J. Z. Ferreira, R. K. Jain and M. S. Sloth, *Inflationary magnetogenesis without the strong coupling problem*, *JCAP* **10** (2013) 004 [1305.7151].

[80] R. Sharma, S. Jagannathan, T. R. Seshadri and K. Subramanian, *Challenges in Inflationary Magnetogenesis: Constraints from Strong Coupling, Backreaction and the Schwinger Effect*, *Phys. Rev. D* **96** (2017) 083511 [1708.08119].

[81] A. Kushwaha and S. Shankaranarayanan, *Helical magnetic fields from Riemann coupling*, *Phys. Rev. D* **102** (2020) 103528 [2008.10825].

[82] A. Kushwaha, A. Naskar, D. Nandi and S. Shankaranarayanan, *Effective field theory of magnetogenesis identify necessary and sufficient conditions*, *JCAP* **01** (2023) 045 [2207.05162].

[83] D. Maity, S. Pal and T. Paul, *Effective Theory of Inflationary Magnetogenesis and Constraints on Reheating*, *JCAP* **05** (2021) 045 [2103.02411].

[84] S. Tripathy, D. Chowdhury, R. K. Jain and L. Sriramkumar, *Challenges in the choice of the nonconformal coupling function in inflationary magnetogenesis*, *Phys. Rev. D* **105** (2022) 063519 [2111.01478].

[85] A. Brandenburg, O. Iarygina, E. I. Sfakianakis and R. Sharma, *Magnetogenesis from axion-SU(2) inflation*, 2408.17413.

[86] C. J. Hogan, *Magnetohydrodynamic effects of a first-order cosmological phase transition*, *Phys. Rev. Lett.* **51** (1983) 1488.

[87] J. M. Quashnock, A. Loeb and D. N. Spergel, *Magnetic Field Generation during the Cosmological QCD Phase Transition*, *Astrophys. J. Lett.* **344** (1989) L49.

[88] T. Vachaspati, *Magnetic fields from cosmological phase transitions*, *Phys. Lett. B* **265** (1991) 258.

[89] G. Baym, D. Bodeker and L. D. McLerran, *Magnetic fields produced by phase transition bubbles in the electroweak phase transition*, *Phys. Rev. D* **53** (1996) 662 [hep-ph/9507429].

[90] G. Sigl, A. V. Olinto and K. Jedamzik, *Primordial magnetic fields from cosmological first order phase transitions*, *Phys. Rev. D* **55** (1997) 4582 [astro-ph/9610201].

[91] R. Durrer and A. Neronov, *Cosmological Magnetic Fields: Their Generation, Evolution and Observation*, *Astron. Astrophys. Rev.* **21** (2013) 62 [1303.7121].

[92] K. Subramanian, *The origin, evolution and signatures of primordial magnetic fields*, *Rept. Prog. Phys.* **79** (2016) 076901 [1504.02311].

[93] T. Vachaspati, *Progress on cosmological magnetic fields*, *Rept. Prog. Phys.* **84** (2021) 074901 [2010.10525].

[94] A. Brandenburg and N. N. Protiti, *Electromagnetic Conversion into Kinetic and Thermal Energies*, *Entropy* **25** (2023) 1270 [2308.00662].

[95] A. Brandenburg, K. Enqvist and P. Olesen, *Large-scale magnetic fields from hydromagnetic turbulence in the very early universe*, *Phys. Rev. D* **54** (1996) 1291 [astro-ph/9602031].

[96] M. Christensson, M. Hindmarsh and A. Brandenburg, *Inverse cascade in decaying three-dimensional magnetohydrodynamic turbulence*, *Phys. Rev. E* **64** (2001) 056405.

[97] R. Banerjee and K. Jedamzik, *The Evolution of cosmic magnetic fields: From the very early universe, to recombination, to the present*, *Phys. Rev. D* **70** (2004) 123003 [astro-ph/0410032].

[98] A. Brandenburg and T. Kahniashvili, *Classes of hydrodynamic and magnetohydrodynamic turbulent decay*, *Phys. Rev. Lett.* **118** (2017) 055102 [1607.01360].

[99] P. Adshead, J. T. Giblin, T. R. Scully and E. I. Sfakianakis, *Gauge-preheating and the end of axion inflation*, *JCAP* **12** (2015) 034 [1502.06506].

[100] M. Zhou, P. Bhat, N. F. Loureiro and D. A. Uzdensky, *Magnetic island merger as a mechanism for inverse magnetic energy transfer*, *Phys. Rev. Res.* **1** (2019) 012004 [1901.02448].

[101] P. Bhat, M. Zhou and N. F. Loureiro, *Inverse energy transfer in decaying, three-dimensional, non-helical magnetic turbulence due to magnetic reconnection*, *Mon. Not. Roy. Astron. Soc.* **501** (2021) 3074 [2007.07325].

[102] D. N. Hosking and A. A. Schekochihin, *Reconnection-Controlled Decay of Magnetohydrodynamic Turbulence and the Role of Invariants*, *Phys. Rev. X* **11** (2021) 041005 [2012.01393].

[103] D. N. Hosking and A. A. Schekochihin, *Cosmic-void observations reconciled with primordial magnetogenesis*, *Nature Commun.* **14** (2023) 7523 [2203.03573].

[104] A. Brandenburg, A. Neronov and F. Vazza, *Resistively controlled primordial magnetic turbulence decay*, *Astron. Astrophys.* **687** (2024) A186 [2401.08569].

[105] A. A. Schekochihin, *MHD turbulence: a biased review*, *J. Plasma Phys.* **88** (2022) 155880501 [2010.00699].

[106] W. H. Press and P. Schechter, *Formation of Galaxies and Clusters of Galaxies by Self-Similar Gravitational Condensation*, *The Astrophysical Journal* **187** (1974) 425.

[107] A. M. Green, A. R. Liddle, K. A. Malik and M. Sasaki, *New calculation of the mass fraction of primordial black holes*, *Phys. Rev. D* **70** (2004) 041502.

[108] C. T. Byrnes, E. J. Copeland and A. M. Green, *Primordial black holes as a tool for constraining non-Gaussianity*, *Phys. Rev. D* **86** (2012) 043512 [1206.4188].

[109] J. Schwinger, *On gauge invariance and vacuum polarization*, *Phys. Rev.* **82** (1951) 664.

[110] M. B. Fröb, J. Garriga, S. Kanno, M. Sasaki, J. Soda, T. Tanaka and A. Vilenkin, *Schwinger effect in de Sitter space*, *JCAP* **04** (2014) 009 [1401.4137].

[111] T. Kobayashi and N. Afshordi, *Schwinger Effect in 4D de Sitter Space and Constraints on Magnetogenesis in the Early Universe*, *JHEP* **10** (2014) 166 [1408.4141].

[112] R. Sharma and S. Singh, *Multifaceted Schwinger effect in de Sitter space*, *Phys. Rev. D* **96** (2017) 025012 [1704.05076].

[113] T. Fujita, J. Kume, K. Mukaida and Y. Tada, *Effective treatment of U(1) gauge field and charged particles in axion inflation*, *JCAP* **09** (2022) 023 [2204.01180].

[114] R. von Eckardstein, K. Schmitz and O. Sobol, *On the Schwinger effect during axion inflation*, 2408.16538.

[115] A. Roper Pol, A. Brandenburg, T. Kahniashvili, A. Kosowsky and S. Mandal, *The timestep constraint in solving the gravitational wave equations sourced by hydromagnetic turbulence*, *Geophys. Astrophys. Fluid Dyn.* **114** (2020) 130 [1807.05479].